Report
P-18-16
February 2019

Full-scale test of the Dome Plug for KBS-3V deposition tunnels – concrete properties

Sampling, testing and properties of low-pH concrete in the KBP1016 dome plug

Carsten Vogt

SVENSK KÄRNBRÄNSLEHANTERING AB

SWEDISH NUCLEAR FUEL
AND WASTE MANAGEMENT CO

Box 3091, SE-169 03 Solna
Phone +46 8 459 84 00
skb.se

SVENSK KÄRNBRÄNSLEHANTERING

ISSN 1651-4416
SKB P-18-16
ID 1689616
February 2019

Full-scale test of the Dome Plug for KBS-3V deposition tunnels – concrete properties

Sampling, testing and properties of low-pH concrete in the KBP1016 dome plug

Carsten Vogt, Betong & Stålteknik

Keywords: Dome plug, Low-pH concrete, Material properties, Destructive testing.

Abstract

The disposal of spent nuclear fuel in copper canisters according to the KBS-3V method is proposed by SKB. The radioactive waste is contained by engineered barriers and the host rock. The canisters are placed in vertical deposition holes in horizontal deposition tunnels. The deposition tunnels are back-filled with bentonite and closed with a deposition tunnel plug. This plug is designed as an unreinforced concrete dome plug, consisting of a special concrete mix (low-pH concrete). A low-pH concrete contains high amounts of amorphous silica in the cementitious binder in order to lower the pH of the cement paste.

The system design of the dome plug was carried out in an earlier project (KBP1004). The plug system was designed and verified with calculations, laboratory experiments and different scale tests. Installing and testing the full-scale plug system under realistic conditions at 450 m depth in the Äspö Laboratory was a crucial part of this earlier project.

After 5 years of monitoring the plug, the KBP1016 project takes over. The main objective of KBP1016 is to dismantle and evaluate the full-scale plug which was installed in KBP1004. The evaluation will be done before, during and after the dismantling itself, using tests, analyses and sampling. One of the project aims is to propose improvements to be used as a basis for future design. The dome plug was subjected to tests on gas tightness and a test of the load bearing capacity with 8 MPa water pressure (stress test) prior to dismantling (total pressure including the swelling pressure from the bentonite was > 9 MPa). Non-destructive testing of the structural integrity and extraction of samples for the determination of concrete properties was performed. The maturity and properties of the bentonite seal and backfill behind the plug were investigated.

This report summarizes the quality and properties of the low-pH concrete in the dome plug after the final experiments which were performed prior to dismantling. Visual inspection of drill cores and laboratory investigations were performed.

No obvious defects like cracks, honeycombing or large voids were found in the concrete itself. However, the slot in the upper part of the plug was not completely filled with concrete. A triangular void with a height of approximately 50 cm was never filled with concrete or grout. The interface between the rock and the concrete was filled with grout. The amount of grout between the rock and the concrete increased with increasing height in the plug, indicating an increased gap width prior to grouting in the upper parts.

A certain bond strength between the concrete and the rock/grout must exist. This was shown on the drill cores in the interface between the concrete and the rock because these cores did not fall apart when extracting the drill cores. The actual value for the bond strength could only be measured on one sample in the laboratory. No value for the bond strength between the concrete and the rock could be obtained in the in situ tests either. One obvious reason was that the samples were situated too close to a grouting pipe with steel fixation and protective geotextile, thus breaking the bond. However, the overall view suggests that there is a certain bond between the concrete and the rock. The bond is inconsistent with partly low bond strength and partly no measurable strength at all.

Most of the mechanical properties investigated were on average comparable with undisturbed samples from earlier tests and samples from the monolith cast beside the plug. This indicates that aging, loading and restrained shrinkage had only a limited influence on the mechanical properties of the low pH concrete.

There are indications that the concrete may have been influenced negatively in certain areas. The compressive strength was lower close to the surfaces of the plug and the average tensile strength appears to be somewhat lower than results from earlier tests. The permeability of the tested concrete samples is higher in the upper parts and close to the downstream surface. These observations coincide with results from investigations of the microstructure.

The investigations of the microstructure revealed more microcracks close to the surface of the plug. This may originate from loading or restrained shrinkage and correlates with certain results from tests on the mechanical properties. The reason for the existence of a surface layer with increased porosity

could not be exactly determined. The possibility that leaching or carbonation has caused this layer with high porosity is deemed unlikely. The most plausible explanation is that the high porosity in the surface layer was caused during pouring of the concrete or insufficient curing. The chemical analysis of the paste showed that chlorides penetrated unevenly from the downstream surface, the depth of penetration varies between 10 mm and 40 mm. The determined CaO/SiO_2 ratio is higher than values determined in Vogt et al. (2009) and also higher than the theoretical value of ca 0.75, presumably due to the incorporation of limestone filler in the analysis. The determined pH value by leaching tests is consistent with earlier investigations on laboratory samples. Thus, the composition of the C-S-H in the low-pH concrete from the plug should, in all probability, be similar to those found in laboratory samples.

The comparison of stipulated values for material properties for structural calculations from earlier laboratory tests (see Vogt et al. 2009 and Grahm et al. 2015) with tested values shows that the concrete in the plug is consistent with most of the anticipated parameters with the exception of tensile strength. It should be noted that the concrete was subjected to severe loading and quick unloading, as well as restrained shrinkage which may have resulted in microcracking. This was confirmed by investigations of the microstructure.

Possible improvements

One of the most important observations made while investigating and dismantling the dome plug was that the top part of the slot was not filled with concrete. Since grouting was terminated before this void was filled with grout, a triangular void with a height of approximately 50 cm remained. It is mpressive that the dome plug performed as expected, despite this defect. In future production, this type of defect shall be avoided.

There are several possible solutions to this problem. For the highest chance of success, a combination of several measures should be used.

- Install cameras, sensors or similar on top of the slot in order to ensure that pumping is not terminated before the slot is completely filled.
- Increase the number and diameter of venting pipes at the top of the slot. Observe that these pipes have to be removed when casting is finished since they may provide possible leakage passageways.
- Cast the top part of the plug (into the slot) with a modified concrete mix design. The amount of coarse aggregate could be reduced and the dosage of superplasticizer increased for enhanced flowability of the low-pH concrete. This should simplify complete filling of the slot.
- Place one or more extra pumping pipe(s) at the top of the slot. Observe that these pipes need to be removed when casting is finished since they may provide possible leakage passageways. Venting pipes are required.
- Drill one or more holes from the downstream side of the plug through the rock to the top of the slot. Cast the last part of the plug from the top of the slot. The drilled hole is to be filled with concrete once the plug is finished. Venting pipes are required.
- Allow for increased grouting in order to fill voids. This should be seen as a last resort instead of having to replace a faulty plug. Dismantling a faulty plug and constructing a new plug possibly also includes having to remove and replace the bentonite in the barrier.

Sammanfattning

Deponering av förbrukat kärnbränsle i kopparkapslar enligt KBS-3V-metoden föreslås av SKB. Det radioaktiva avfallet innesluts av tekniska barriärer och urberget. Behållarna placeras i vertikala deponeringshål i horisontella deponeringstunnlar. Deponeringstunnlarna fylls med bentonit och stängs med en pluggkonstruktion. Denna plugg är konstruerad som en oarmerad betongkupol, bestående av en särskild betongblandning (låg-pH-betong). En låg-pH-betong innehåller höga mängder amorft kiseldioxid i bindemedlet för att sänka cementpastans pH-värde.

Systemdesignen av kupolpluggen utfördes i ett tidigare projekt (KBP1004). Pluggen konstruerades och verifierades med beräkningar, laboratorieexperiment och olika skaltest. Installering och provning av ett fullskaligt pluggsystem under realistiska förhållanden vid 450 m djup i Äspölaboratoriet var en viktig del av detta tidigare projekt.

Efter 5 års övervakning av pluggen tar KBP1016-projektet över. Huvudsyftet med KBP1016 är att bryta och utvärdera den fullskaliga pluggen som installerades i KBP1004. Utvärderingen kommer att utföras före, under och efter brytningen, med hjälp av tester, analyser och provtagning. Ett av projektets mål är att föreslå förbättringar som ska användas som grund för framtida design. Kupolpluggen utsattes för prov på gastäthet och ett test av bärförmågan med 8 MPa vattentryck (stress test) före brytning (totaltrycket inklusive svälltrycket var > 9 MPa). Icke-förstörande provning av pluggens integritet och uttag av prover för bestämning av betongegenskaper utfördes. Mognad och egenskaper hos bentonittätningen och fyllningen bakom pluggen undersöktes.

Denna rapport sammanfattar egenskaperna hos låg-pH-betongen i kupolpluggen efter de slutliga experimenten som utfördes före brytning. Visuell inspektion av borrkärnor och olika laboratorie-undersökningar utfördes.

Inga uppenbara defekter som sprickor, ballastansamlingar eller stora hålrum hittades i själva betongen. Slitsen i den övre delen av pluggen var dock inte helt fylld med betong. Ett triangulärt hålrum med en höjd av cirka 50 cm fylldes aldrig med betong eller injekteringsbruk. Övergångszonen mellan berget och betongen fylldes med injekteringsbruk. Mängden bruk mellan berg och betong ökade med ökande höjd i pluggen.

En viss vidhäftning mellan betong och berg/injekteringsbruk måste ha funnits. Detta visades på borrkärnorna i övergångszonen mellan betong och berg, eftersom dessa kärnor inte ramlade isär vid uttag av borrkärnorna. Det faktiska värdet för vidhäftningshållfastheten kunde endast mätas på ett prov i laboratoriet. Inget värde för vidhäftningshållfasthet mellan betong och berg kunde erhållas i testerna på plats. En anledning var att proverna var placerade för nära en injekteringsslang med stålfixering och skyddande geotextil, vilket störde vidhäftningen. Den övergripande bedömningen är att en viss vidhäftning mellan betong och berg finns. Vidhäftningen varierar dock med delvis låga värden och delvis ingen mätbar styrka alls.

De flesta av de undersökta mekaniska egenskaperna hos betongen var i genomsnitt jämförbara med ostörda prov från tidigare tester. Detta indikerar att ingen dramatisk försämring av låg-pH betongens mekaniska egenskaper skedde på grund av åldring, pålastning och förhindrad krympning.

Det finns tecken på att betongen kan ha påverkats negativt i vissa områden. Tryckhållfastheten var lägre i närheten av pluggens ytor och den genomsnittliga draghållfastheten verkar vara något lägre än resultaten från tidigare test. Permeabiliteten hos de testade betongproverna är högre i de övre delarna och nära nedströmsytan. Dessa observationer stämmer överens med resultat från undersökningar av mikrostrukturen.

Undersökningarna av mikrostrukturen visade ett ökat antal mikrosprickor nära pluggen yta. Detta kan vara orsakad av belastning eller förhindrad krympning och korrelerar med vissa resultat från tester av de mekaniska egenskaperna. Orsaken till förekomsten av ett ytskikt med ökad porositet kunde inte exakt bestämmas. Det anses osannolikt att urlakning eller karbonatisering har orsakat detta skikt med hög porositet. Den mest troliga förklaringen är att den höga porositeten i ytskiktet orsakades under gjutningen av betongen eller beror på ofullständig härdning. Den kemiska analysen av cementpastan visade

ojämn kloridinträngning från nedströmssidan, inträngningsdjupet varierade mellan 10 mm och 40 mm. Den bestämda CaO/SiO_2 kvoten är högre än värdena som redovisas i Vogt et al. (2009) och också högre än det teoretiska värdet av cirka 0.75, förmodligen på grund av att kalkstensfiller inkluderades i analysen. PH-värdet som bestämdes genom lakningstest är jämförbart med tidigare undersökningar på laboratorieprover. Således skulle sammansättningen av C-S-H i låg-pH-betongen från pluggen vara sannolikt lik den som finns i laboratorieprover.

Jämförelsen av föreslagna värden för materialegenskaper för bärighetsberäkningar från tidigare laboratorieundersökningar (se Vogt et al. 2009 och Grahm et al. 2015) och testade värden visar att betongen i pluggen överensstämmer för de flesta parametrarna. Ett undantag är draghållfastheten. Det bör noteras att betongen utsattes för höga belastningar och snabb avlastning, såväl som förhindrad krympning, vilket kan ha resulterat i uppkomst av mikrosprickor. Detta bekräftades genom undersökningar av mikrostrukturen.

Möjliga förbättringar

En av de viktigaste observationerna som gjordes vid undersökning och brytning av pluggen var att den övre delen av slitsen inte fylldes helt med betong. Eftersom injekteringen avbröts innan detta tomrum fylldes med injekteringsbruk kvarstod ett triangulärt tomrum med en höjd av cirka 50 cm. Det är förvånansvärt att kupolpluggen fungerade som förväntat, trots denna defekt. Vid framtida produktion ska denna typ av fel undvikas.

Det finns flera möjliga lösningar på detta problem. En kombination av flera åtgärder bör användas för ökad säkerhet.

- Installation av kameror, sensorer eller liknande i toppen av slitsen för att säkerställa att pumpningen inte avbryts innan slitsen är full.
- Ökat antal och diameter för avluftningsrören högst upp i slitsen. Observera att dessa rör måste avlägsnas när gjutningen är klar eftersom de kan resultera i eventuella läckagevägar.
- Gjuta den övre delen av pluggen (i slitsen) med ett modifierat betongrecept. Mängden grovballast kan reduceras och dosen av flytmedel ökas för ökad flytförmåga hos låg-pH-betongen. Detta borde förenkla fullständig fyllnad av slitsen.
- Placering av ett eller flera extra pumprör i toppen av slitsen. Observera att dessa rör måste avlägsnas när gjutningen är klar eftersom de kan ge eventuella läckagevägar. Avluftningsrör krävs.
- Borrning av ett eller flera hål från pluggens nedströmssida genom berget till toppen av slitsen. Gjutning av pluggen sista del från toppen av slitsen genom dessa hål. Det borrade hålet måste fyllas med betong när gjutning av pluggen är klar. Avluftningsrör krävs.
- Tillstånd för ökad mängd injekteringsbruk för att fylla eventuella tomrum. Detta bör ses som en sista utväg istället för rivning av en plugg.

Contents

1 Introduction

1.1 Background

“The KBS-3V method is proposed by SKB for the disposal of spent fuel packaged in copper canisters with cast iron inserts in a crystalline host rock. The long-term safety principles are based on isolation and containment of radioactive waste through the choice of a stable geological environment at depth and the use of a multi-barrier system consisting of engineered barriers (canister, buffer, backfill, and closure) and the host rock. The canisters are emplaced in vertical holes, containing pre-compacted blocks of bentonite buffer, below horizontal deposition tunnels. The deposition tunnels are backfilled with bentonite blocks and pellets and closed with a deposition tunnel plug” (Grahm et al. 2015).

System design of the dome plug intended to seal the deposition tunnels was carried out in the previous project KBP1004-System design of dome plug for deposition tunnels 2010–2015. The development and verification of the plug system has been carried out with analytical and numerical calculations, laboratory experiments and different scale-tests. The most significant activity in the project was to test the full-scale plug system under realistic geohydrological conditions at 450 m depth in the Äspö Laboratory.

A crucial goal of the full-scale test was to demonstrate that a full-scale plug can be installed in the final repository environment. During the installation, it was necessary to verify practical construction aspects such as concrete deliveries, logistics and health and safety and to verify the results of the work performed.

Another basic purpose of the experiment was to measure the waterproofing ability of the plug after installation. The dome plug has therefore been subjected to a high water pressure of 4 MPa (about 40 bar). This pressure corresponds to an expected maximum groundwater pressure in the nuclear fuel repository during the operating period and closure phase. However, it remains to evaluate the function of the plug as well as to analyze whether the performed modeling/calculations are consistent with observations made during and after dismantling.

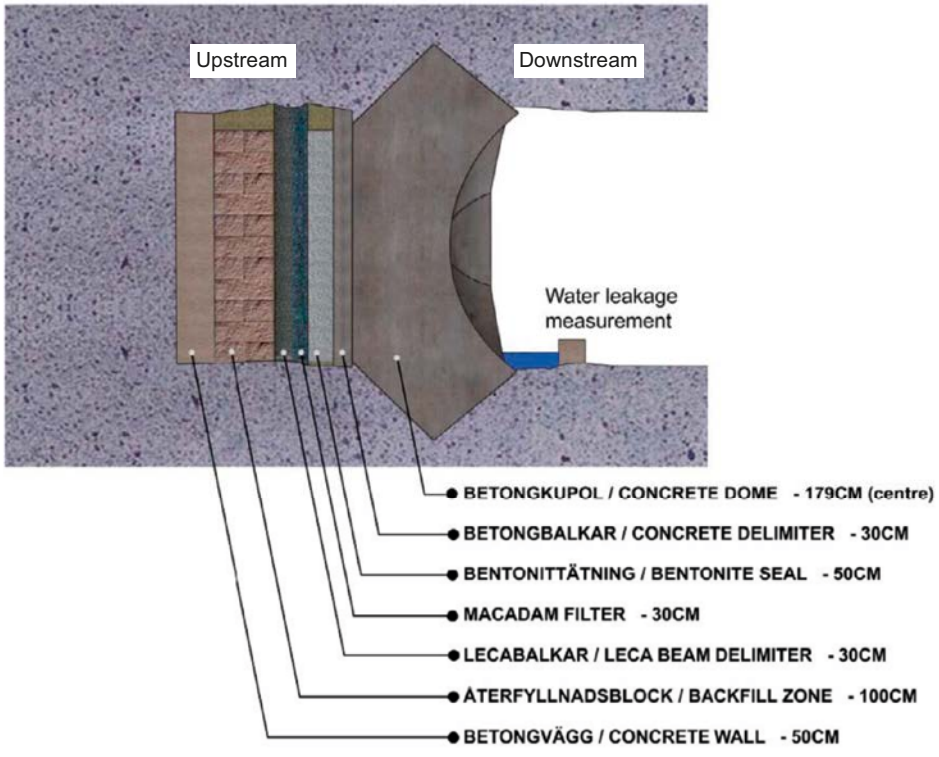

Figure 1-1. *Schematic section of the DOMEPLU full-scale test, from Grahm et al. (2015).*

The dome plug was installed in spring 2013 and since then, more than 100 sensors have monitored the construction. This part of the experiment was completed in 2017 when a new phase of the full-scale trial was initiated with the KBP1016 project "Dismantling and evaluation of the dome plug". In these experiments, the plug was tested for gas tightness and it was exposed to a load of approximately 8 MPa (stress test).

The main objective of KBP1016 is to dismantle and evaluate the full-scale casting which was installed in KBP1004. The evaluation will be done before, during and after the actual dismantling, using tests, analyses and sampling. One of the aims of the project is to propose improvements that can be used as a basis for future design.

1.2 Purpose and content of the report

This report summarizes the sampling, testing and test results of the low-pH concrete in the experimental dome plug (DOMEPLU), installed at 450 m depth in the Äspö laboratory.

The experimental data also contains results regarding compressive strength and creep in compression from experiments started in the now terminated low-pH concrete project (KBP5001).

1.3 Limitations

This report summarizes results of material properties presented in test reports from laboratories. The correctness of the individual results or test methods depends on the laboratory. However, it is checked if the obtained results are reasonable.

This report is part of a series of reports and thus, it is not intended to be read separately. This report does not include a complete description of all performed experiments in the KBP1016 project and their results. These are reported elsewhere. It is not the intention or purpose of this report to discuss and/or evaluate the function of the dome plug in general.

1.4 Orientation

The major goal of the KBP1016 project is to dismantle and evaluate the full-scale dome plug which was installed in the KBP1004 project. One part of the evaluation is to compare the properties of the low-pH concrete in the full-scale plug with the pre-determined values from laboratory and small-scale experiments. The latter having been used in the design phase of the dome plug. Also, undisturbed samples from a monolith cast beside the plug are used for comparison. The concrete in the monolith was mixed on the same day and cast together with the plug. It was exposed to the same environment but not loaded by water pressure. Thus, it may serve as a source for undisturbed samples.

The mechanical properties as well as certain aspects related to durability of the low-pH concrete are compared with the design values. The concrete has been exposed to severe loading for several years. Observe that the relatively short exposure time to the environment of the Äspö tunnels may only hint on durability problems since both environment and exposure time differ from the final installation. The material parameters characterizing the low-pH concrete are summarized in Table 1-1. These parameters were used for calculations and simulations of the structural integrity and performance of the dome plug. The values in Table 1-1 are recalculated to characteristic values from various laboratory tests.

Table 1-1. Material parameters used for the design of the dome plug, from Grahm et al. (2015).

Material parameter	Order of magnitude
Compressive strength f_{ck}	54 MPa (90d, cylinder)
Tensile strength f_{ctk}	2.9 MPa
E-modulus E_{cm}	34 GPa
Density	2336 kg/m^3
Other important properties	
Permeability coefficient K	10^{-11} m/s

In order to be able to evaluate the material properties of the low-pH concrete, a certain number of drill cores were taken from the dome plug before dismantling. The following properties were determined and are used for evaluation:

- Bond strength between rock and concrete or rock and grout at the interface between concrete and rock. Gap width and/or thickness of injection grout at the interface zone.
- Compressive strength and tensile strength.
- E-modulus.
- Permeability.
- Moisture properties (degree of capillary saturation).
- Carbonation, homogeneity, microstructure and chemical composition of the low-pH concrete.

Drill cores for laboratory testing were taken at predefined positions and testing of the bond strength was also performed in situ. This test had to be performed after dismantling the plug since the downstream surface of the slot in the rock was not accessible earlier.

2 Sampling

2.1 Type and position of drill cores

Drilling was done according to a predetermined schedule. However, certain adjustments had to be done during dismantling, see also later sections of this report. The drill cores in the interface between rock and concrete have a diameter of approximately 150 mm. In situ testing of bond strength is usually performed on 50–70 mm cores. All other drill cores have a diameter of approximately 95 mm (using a 100 mm drill). Figure 2-1 to Figure 2-4 show the position of the drill cores and in situ testing on the plug.

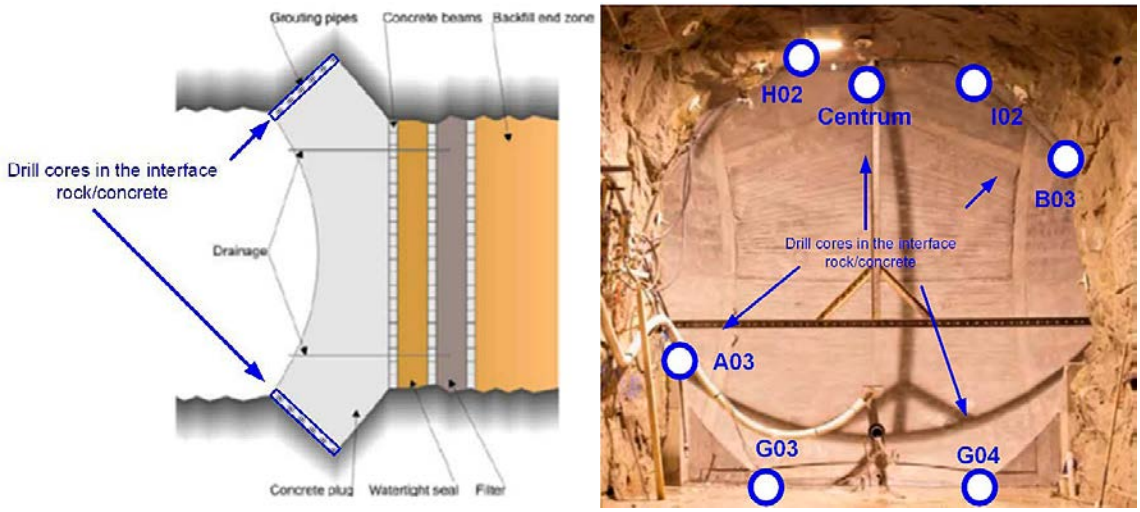

Figure 2-1. *Drill cores with diameter 150 mm for investigation of the interface between rock and concrete.*

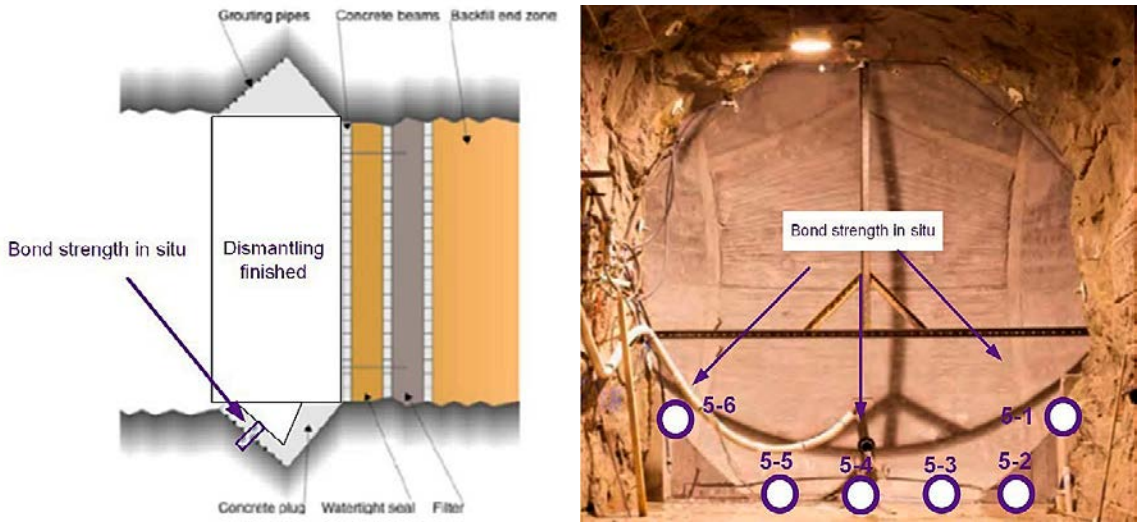

Figure 2-2. *In situ test of bond strength between rock and concrete on the upstream face of the slot in the rock.*

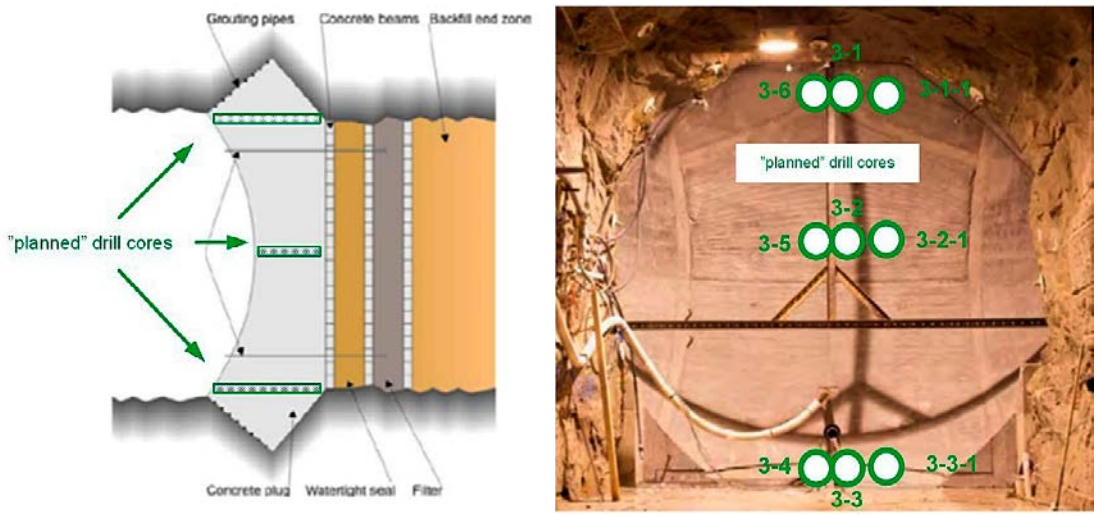

Figure 2-3. *Drill cores with diameter 95 mm for material testing.*

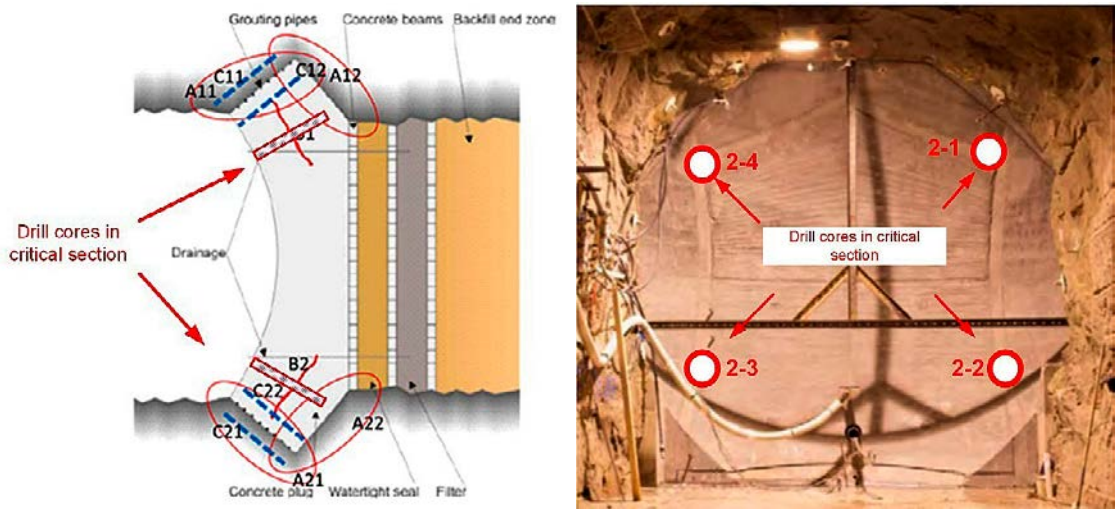

Figure 2-4. *Drill cores with diameter 95 mm in the critical section (high tensile stresses).*

2.2 Observations during sampling/drilling

While drilling the 150 mm cores in the upper part of the plug (H02 and I02 in Figure 2-5), a layer of grout (approximately 20 cm thick) was observed in the top part of the cores. A void on top of the grout was observed when video filming the drilled holes, i.e. it was confirmed that the slot above the grout is empty to the very top.

Obviously, the slot was not completely filled with concrete while casting. This also explains why more material than calculated was used when grouting the interface between rock and concrete after the second cooling procedure (see Grahm et al. 2015).

Therefore, an additional core was taken in the center of the upper part of the plug (denoted center in Figure 2-6). This core showed the same situation, a layer of grout on top of the low-pH concrete. After dismantling the plug, it was confirmed that the top part is empty and the concrete has an almost horizontal top under a layer of grout, see Figure 2-6. A triangular shape of the slot with a height of about 50 cm was never filled with concrete. It would have required almost one m^3 of grout to fill this void.

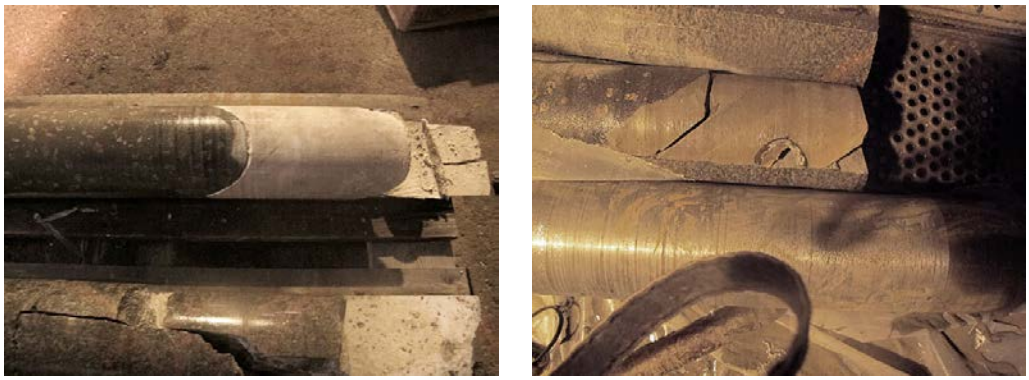

Figure 2-5. *Drill cores H02 (left) and I02 (right). The top part of the cores is displayed.*

Figure 2-6. *Drill core "center" (left) and void on top of the concrete (right).*

2.3 Photo-documentation of drill cores

2.3.1 Drill cores in the interface

Below, some of the drill cores are shown. All photographs can be found in Appendix. All comments are only valid for the downstream side of the plug. For most cores, a certain amount of grout in between concrete and rock is visible and the concrete had a certain bond to the rock/grout, see Figure 2-7.

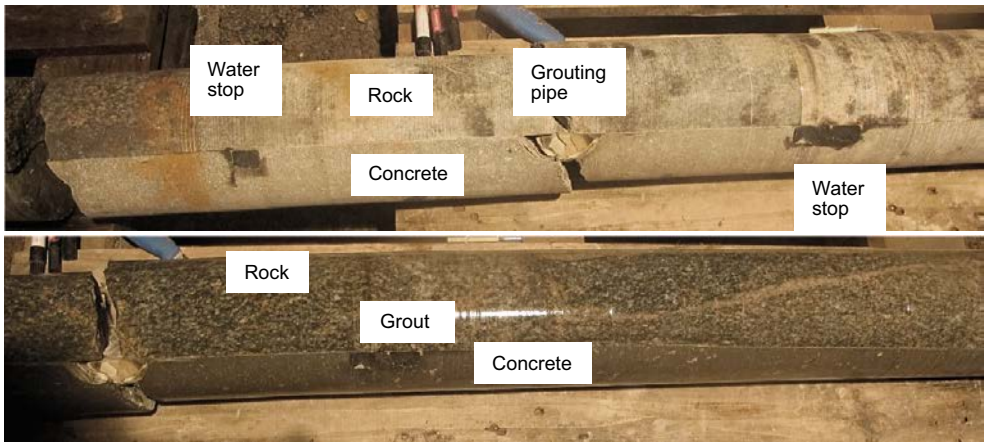

Figure 2-7. *Examples of drill cores (A03) from the interface between rock and concrete immediately after drilling. The water stops (dark squares) and grouting pipes (light colored halve-circles) are clearly visible. Also, a thin layer of grout (light color) at the interface. These cores seemed to be attached to each other after drilling, i.e. a certain bond strength existed.*

Downstream of the water stops, no grout was observed. The water stops efficiently stopped the grout from penetrating to the downstream surface. The initial placement of grouting pipes and water stops is explained in Grahm et al. (2015). In certain cores, smaller amounts of grout had penetrated the interface, see Figure 2-8. These cores are located in the lower part of the plug. More grout appears to have penetrated between rock and concrete at the upper part of the plug and at the sides.

After arrival at the laboratory and sampling, the concrete had detached from the rock for most cores, see Figure 2-9.

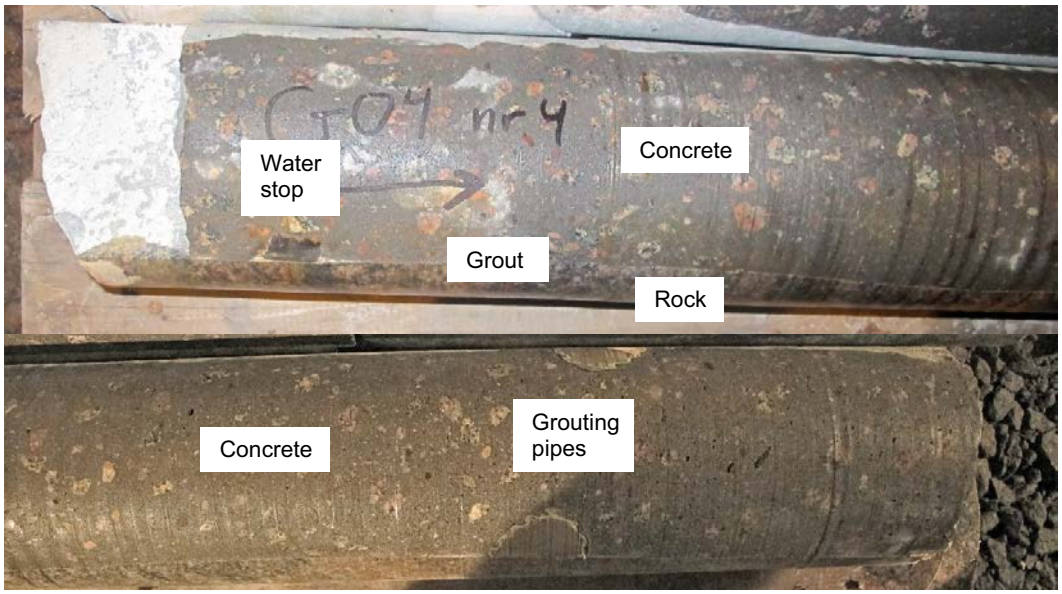

Figure 2-8. *Examples of drill cores (G04) from the interface between rock and concrete immediately after drilling. The water stops (dark squares) and grouting pipes (light colored halve-circles) are clearly visible. Very little or almost no grout seems to have penetrated at the interface. These cores seemed to be attached to each other after drilling, i.e. a certain bond strength existed.*

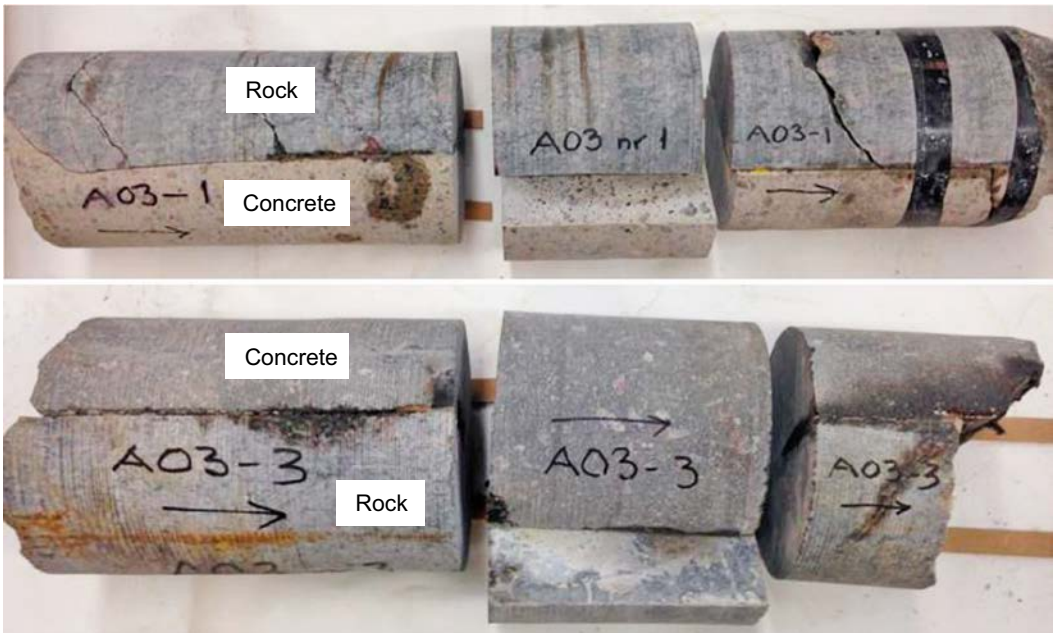

Figure 2-9. *Examples of drill cores (A03) from the interface between rock and concrete after arrival at the laboratory and sampling. The concrete came loose from the rock in almost all samples, i.e. little or no bond strength existed.*

2.3.2 Drill cores in the plug

Below, some of the drill cores are documented in photographs. All photographs can be found in Appendix. In general, the cores show very homogenous concrete with evenly distributed coarse aggregates, see Figure 2-10. Cooling pipes and cables from the instrumentation are very well embedded. No visible cracks or any form of honeycombing are observed. However, in certain parts of the cores, locally there are reduced amounts of coarse aggregate, see Figure 2-11 in comparison with Figure 2-10. This observation may be a result of "sieving out" the coarse aggregate by cooling pipes and other installations and thus, a certain segregation of concrete. Another kind of segregation also occurs sometimes in the concrete trucks itself, especially when delivering self-compacting concrete. The very last concrete in the drum tends to lack coarse aggregate, especially if unloading took a long time. It seems to be a localized phenomenon, since it was not observed on cores 3-3 and 3-4, situated right next to core 3-3-1.

Figure 2-10. *Core 3-3-1, part 2. The large aggregates seem very well distributed, the cooling pipe is well embedded in concrete.*

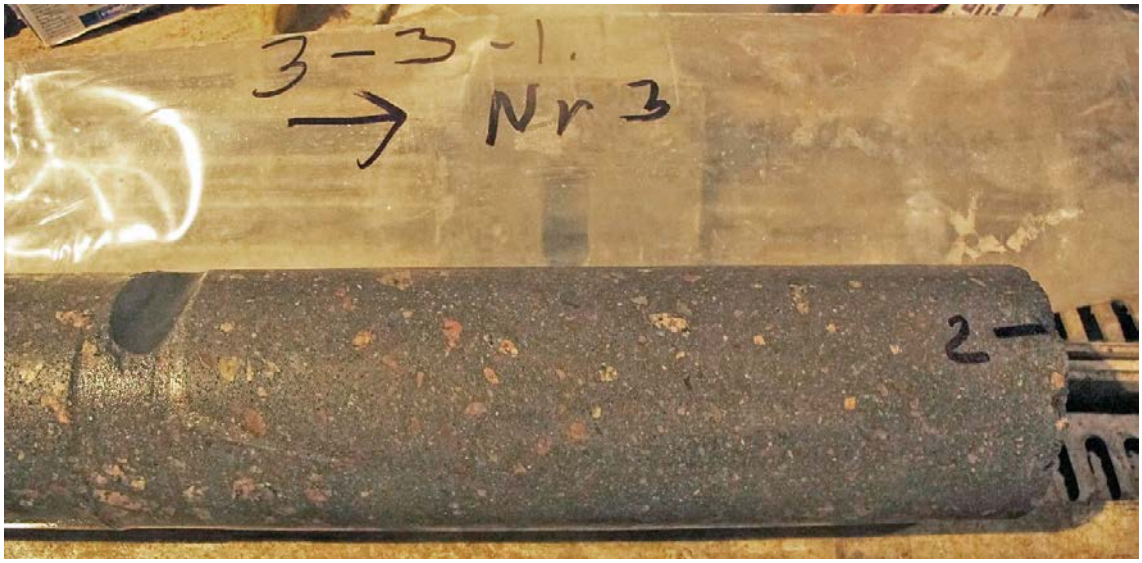

Figure 2-11. *Core 3-3-1, part 3. This part of the core shows a lower content of coarse aggregate.*

2.3.3 Drill cores from in situ test of bond strength

Below, some of the drill cores are documented in photographs. All photographs can be found in Appendix. In all drill cores there are residues from grouting pipes, the stainless-steel profile from fixing the grouting pipes to the rock or the geotextile protecting the grouting pipes.

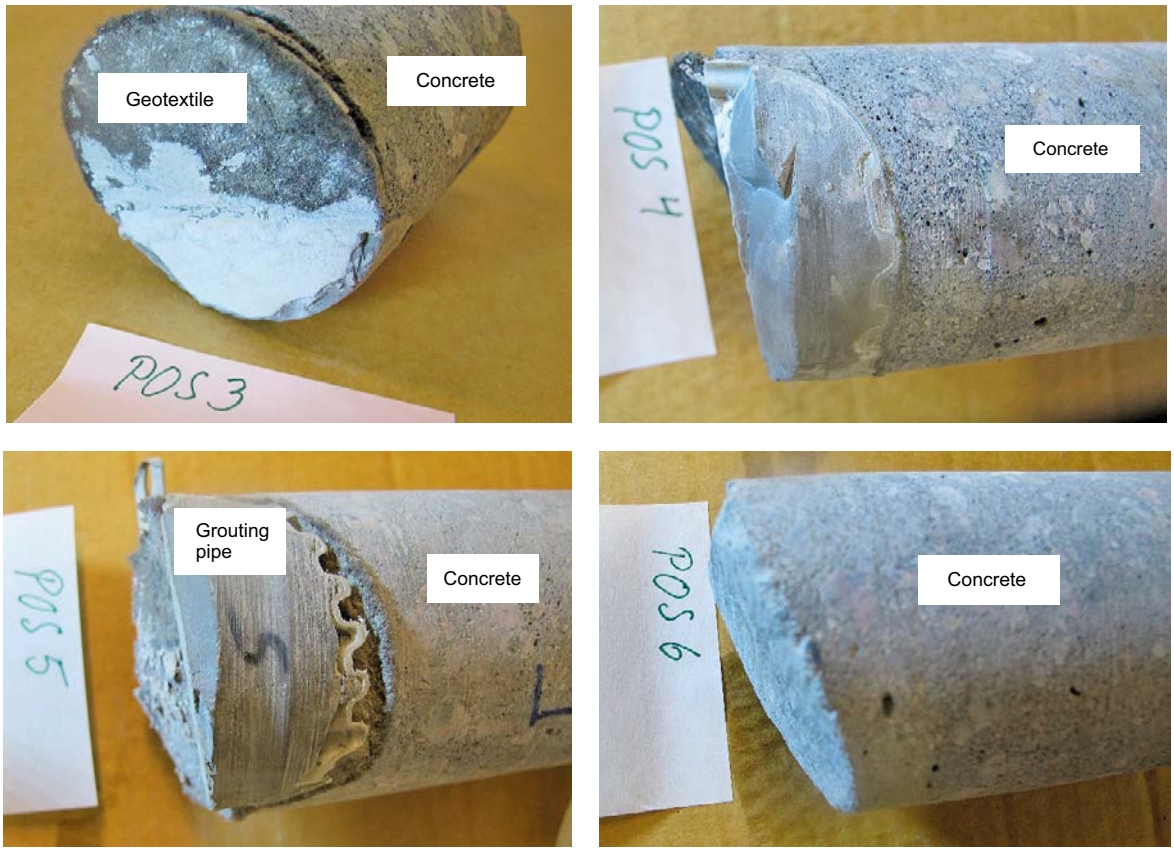

Figure 2-12. *Drill cores from in situ test of bond strength. The geotextile covering the grouting pipes or the grouting pipes itself are clearly visible.*

3 Testing

Different test methods were used to characterize the properties of the low-pH concrete after the dome plug experiment was completed. Table 3-1 summarizes these tests. The “critical section” is a part of the plug where high tensile strengths were calculated to occur and thus, cracks are probable.

All samples originate from the dome plug that was cast on the 13th of march 2013. The drilling was done in November/December 2017 and testing was done in January/February 2018. So, the samples are about 1 800 days of age at the time of testing.

Table 3-1. Test methods used for different samples and corresponding standards.

Description	Material property	Standard/method
At the interface between concrete and rock		
	Bond strength, using splitting tensile strength test	SS-EN 12390-6
	Visual inspection of the gap and estimation of the amount of grout in the gap	
In the “critical section”		
	Compressive strength	SS-EN 12390-3
	Direct tensile strength	SS 13 72 31
“planned” drillcores		
	Compressive strength	SS-EN 12390-3
	Direct tensile strength	SS 13 72 31
	E-modulus	SS 13 72 32
	Water tightness (permeability)	SS-EN 12390-8
	pH	SKB-method, leaching
	Moisture	Degree of capillary saturation
	Carbonation	pH-indicator and thin section
	Microstructure	SEM microscopy and thin section
“unplanned” drillcores (option)		
	If required	If required
Bond strength between rock and concrete/grout on site		
	Bond strength, site test	SS 13 72 43

3.1 Test methods

The standardized test methods for compressive strength, direct tensile strength, splitting tensile strength, E-modulus, in situ bond strength and water tightness need no further description. All relevant information can be found in the corresponding standards. Below, special test methods are explained in more detail.

3.1.1 Bond strength between rock and concrete/grout by means of splitting tensile strength

Drill cores were taken through the interface between concrete and rock. Pieces with a length equal to the diameter are prepared and tested for splitting tensile strength according to SS-EN 12390-6. The test plane for the splitting test is the interface between rock and concrete.

3.1.2 Permeability

Using the results from the water penetration test according to SS-EN 12390-8 (2000) and a concept presented in Neville (1994), the calculation of the water permeability coefficient is possible. The permeability can be described by:

$$K = \frac{e^2 v}{2ht} \quad (3\text{-}1)$$

where e = measured depth of water penetration in the concrete in meters, h = hydraulic head in meters, t = time under pressure in seconds and v = fraction of volume of concrete occupied by pores, typically between 0.02 and 0.06.

Using the details of SS-EN 12390-8, the input into (Equation. 3-1) is:

hydraulic head h = 50 m

time under pressure t = 259 200 s

pore fraction v = 0.04 (chosen).

3.1.3 Microstructure in thin section and SEM

The structure and porosity of the concrete from the drill cores were analyzed using a polarizing microscope. These structures were compared to normal concretes with known water/cement ratios are used as reference. In order to analyze the structure of the concrete a thin section has to be prepared. A thin section is a specimen that has been polished so thin that light can penetrate it. This means that the structure of the concrete can be analyzed in a polarizing microscope. The thin sections are impregnated with epoxy resin containing fluorescent dye. When analyzed in UV light, one can estimate the porosity of the sample. A porous material will absorb more epoxy/dye.

SEM analysis allows much higher resolution than light microscopy. At the same time, the chemical composition can be analyzed, using energy-dispersive X-ray spectroscopy analysis (EDX). SEM analysis was performed on broken surfaces of drill core pieces.

3.1.4 pH in leaching

The pH of the concrete is determined using an equilibrium leaching test in saline water. Pieces of concrete are drilled/sawn from samples. The saline water is a synthetical water with a similar composition as the deep water at the Forsmark site. The test method has been developed for SKB and is implemented as a reference method.

3.1.5 Degree of capillary saturation

For each sample, a piece of concrete is mechanically extracted (broken not drilled or sawn) from the center of a drill core at the current depth. Samples are weighed immediately after withdrawal. The samples are then placed in a box where the undersides are exposed to water. The samples take up water by means of capillary suction. Measurements of the weight increase are made continuously until equilibrium is reached. Then the samples are dried in an oven of 105 °C until equilibrium is reached. The degree of capillary saturation can then be calculated. The method and references are explained in more detail in Andersson (2018).

4 Results and discussion

4.1 Mechanical properties

4.1.1 Compressive strength

The compressive strength of the low-pH concrete of the plug was determined for the cores from the "critical" section (cores 2-1, 2-2, 2-3 and 2-4) and for cores from the center of the plug at three different heights ("planned" cores 3-1-1, 3-2-1 and 3-3-1). For each core, samples were extracted close to the upstream surface, in the middle and close to the downstream surface. The results are summarized in Table 4-1. The spread of the results is relatively large for compressive strength results. This indicates that there are some significant differences between the individual samples. There is a clear tendency that the samples from the central parts of the plug have a higher compressive strength than samples situated close to the upstream or downstream surface. The average of the samples close to the surface is 69 MPa and the central samples have a strength of 75 MPa. The average for all samples is 71 MPa.

Table 4-1. Compressive strength. Level indicates the distance from the downstream surface. From Kalinowski (2018).

Sample ID	Level (mm)	f_{cc} (MPa)
2-1, T1	10–110	68.8
2-1, T2	830–930	72.6
2-1, T3	1 380–1 480	61.9
2-2, T1	10–110	72.6
2-2, T2	760–860	71.9
2-2, T3	1 340–1 440	74.2
2-3, T1	10–110	75.9
2-3, T2	700–800	77.5
2-3, T3	1 380–1 480	74.4
2-4, T1	10–110	71.2
2-4, T2	680–780	77.7
2-4, T3	1 350–1 450	71.4
Avg. critical section		72.5
3-1.1, T1	70–170	63
3-1.1, T2	850–950	69.3
3-1.1, T3	1 780–1 880	59.8
3-2.1, T1	30–125	71.1
3-2.1, T2	780–875	75.4
3-2.1, T3	1 625–1 720	65.3
3-3.1, T1	30–125	69.4
3-3.1, T3	710–805	77.3
3-3.1, T3	1 645–1 740	62.5
Avg. planned		68.7
Avg.		**70.7**
σ		**5.16**
Avg. surface		**68.7**
Avg. center		**74.5**

The compressive strength result in Magnusson and Mathern (2015) for one-year old samples from the monolith is 74 MPa. In Section 5.1, results for two and three years are 76 MPa and 75 MPa respectively. The average of the compressive strength in the plug is 71 MPa, which is lower than previous results from the monolith. However, the central parts of the plug have similar strengths as the samples from the monolith. It's the samples close to the surface that have lower strength. This is presumably due to occurring stresses from loading and/or restrained shrinkage. Aging phenomena can be excluded since the undisturbed samples from the monolith show no comparable tendency. Influences of different

curing are often a reason for differences in compressive strength in concrete structures. Different curing has been ruled out as a reason since the samples from to the upstream surface are situated at least 25 to 30 cm inside the plug. Additionally, the concrete beams and layer of geotextile ensured adequate curing for the upstream side of the plug.

The compressive strength value stipulated for calculations in Vogt et al. is 54 MPa cylinder strength. A statistical evaluation of the compressive strength in accordance to SS-EN 206 for concrete production (compare Magnusson and Mathern 2015) gives after recalculation to equivalent cylinder strength a characteristical compressive strength value of 50 MPa, see Table 4-2. However, the evaluation according to SS-EN 206 is not normal procedure when evaluating production results. The evaluation according to SS-EN 13791 for test of in situ strength fulfills the required criterion for a cylinder strength of 54 MPa by a large margin.

Table 4-2. Evaluation of compressive strength.

	SS-EN 206	**SS-EN 13791**
Number of samples	21	21
Average of cylinder strength (recalcualated) $f_{m(n),\,is}$ (MPa)	56.5	56.5
Standard deviation s	4.21	4.21
Lowest value $f_{is,\,lowest}$ (MPa)	47.8	47.8
Characteristical compressive strength, cylinder (MPa)	54	
$f_{m(n),\,is} - 1.48 \times s$ (MPa)	50.3 < 54	
$f_{is,\,lowest} + 4$ (MPa)	51.8 < 54	
	Not OK	
Characteristical in situ compressive strength, cylinder (MPa)		54 × 0.85 = 45.9
$f_{m(n),\,is} - 1.48 \times s$ (MPa)		50.3 > 45.9
$f_{is,\,lowest} + 4$ (MPa)		51.8 > 45.9
		OK

4.1.2 Tensile strength

The tensile strength of the low-pH concrete was determined for the cores from the “critical” section (cores 2-1, 2-2, 2-3 and 2-4) and for cores from the center of the plug at three different heights (“planned” cores 3-1-1, 3-2-1 and 3-3-1). For each core, samples were extracted close to the upstream surface, in the middle and close to the downstream surface. Table 4-3 summarizes the results. The spread of the results is quite large; however, no clear tendencies can be observed. Direct tensile strength of concrete is known to be a property with a relatively large spread. The average of the cores from the critical section (2.68 MPa) and the average of the “planned” cores are almost identical (2.54 MPa). Therefore, the results from testing of the direct tensile strength do not directly indicate damage due to tensile stresses in the critical section. Comparing the averages of samples close to the surface of the plug (2.59 MPa) and samples from the central part (2.67 MPa) reveals no obvious differences.

The average of the direct tensile strength in the plug is 2.6 MPa. This is slightly lower than previous results. In Magnusson and Mathern (2015), results of 3.2 MPa are reported, however, these were for different specimen size and concrete with lower air content. The corresponding compressive strength was 82 MPa. In Vogt et al. (2009), 2.9 MPa is recommended as a value for calculations. This was based on test results of 3 MPa after 13 days (compressive strength 45 MPa) and 3.3 MPa after 4 months (compressive strength 88 MPa). Again, the concrete had lower air content and was not subjected to loading. There are no results for direct tensile strength available from the monolith. Comparison with splitting tensile strength is difficult due to conversion problems.

Thus, it seems that the concrete in the plug may have been negatively influenced to a certain degree and in certain areas. If this is a result of ongoing aging or if it is due to loading and/or restrained shrinkage is difficult to answer by looking at the tensile strength alone. However, when comparing the results from testing compressive strength, aging seems unlikely. Observe that there are no values for direct comparison with undisturbed samples from the same mix.

Table 4-3. Direct tensile strength. Level indicates the distance from the downstream surface. From Kalinowski (2018).

Sample ID	Level (mm)	f_t (MPa)
2-1, D1	110–210	2.6
2-1, D2	980–1080	2.95
2-1,D3	1480–1580	3.6
2-2, D1	110–210	2.3
2-2, D2	900–1000	2.85
2-2, D3	1440–1540	2.95
2-3, D1	110–210	2.5
2-3, D2	800–900	2.1
2-3, D3	1480–1580	2.95
2-4, D1	110–210	2.7
2-4, D2	780–880	2.25
2-4, D3	1450–1550	2.35
Avg. critical section		2.68
3-1.1, D1	170–270	2.75
3-1.1, D2	990–1090	1.85
3-1.1, D3	1680–1780	2.4
3-2.1, D1	130–225	2.75
3-2.1, D2	885–980	3.1
3-2.1, D3	1530–1625	2.15
3-3.1, D1	125–220	2.05
3-3.1, D2	805–900	3.6
3-3.1, D3	1550–1645	2.25
Avg. planned		2.54
Avg. total		**2.62**
σ		**0.46**
Avg surface		**2.59**
Avg. center		**2.67**

4.1.3 Bond strength to rock, tested in laboratory and in situ and gap between rock and concrete

Only one test could be performed on drill cores in the laboratory. For all other samples, the concrete detached from the rock either while transporting the samples or preparing for the splitting tensile test. The bond strength could be determined for core B03, part 1 at a distance of about 400 mm from the downstream edge of the slot, see Table 4-4. The result is 1.2 MPa.

The bond strength to the rock was also determined in situ. A surface in the remaining part of the plug was prepared at 6 places at exactly the same angle as the rock surface in the slot. The remaining thickness of concrete was approximately 100–240 mm. A core was drilled through concrete and rock and the concrete part was gripped with a special tool and pulled off. The obtained results are displayed in Table 4-5. The in situ test of the bond strength gave no results. This is at least partly due to the fact that the samples were taken more or less directly on the residue of the grouting pipes.

The width of the injected gap was measured for the cores that arrived at the laboratory with bond between rock and concrete. Table 4-6 displays the results. In general, the (grouted) gap width was between 0.2 and 0.7 mm. No clear correlation regarding increasing gap width with increasing height of the position in the plug could be observed. The gap is larger in the middle of the cores A03 and I02, but not for core B03. This contradicts the visual inspection of the cores where a larger grouted gap was observed for the upper cores.

Table 4-4. Bond strength to the rock on drill cores in the laboratory. Level indicates the distance from the downstream surface.

Sample ID	Level (mm)	$f_{ct,\,sp}$ (MPa)
A03-1	300–450	-
A-03-2	650–1 100	-
A-03-3	1 100–1 560	-
A-03-4	1 560–2 860	-
B03-1	310–460	1.2
B03-2	590–1 190	-
B03-3	1 190–2 100	-
B03-4	2 100–2 720	-
Centrum-1	-	-
Centrum-2	-	-
Centrum-3	-	-
Centrum-4	-	-
G03-1 and 2	-	-
G03-3 and 4	-	-
G04-1 and 2 and 3	-	-
G04 nr 4	-	-
H02 nr 1	-	-
H02 nr 2	-	-
H02 nr 3	-	-
I02-1	-	-
I02-2	-	-

Table 4-5. Bond strength to the rock. Tested in situ.

Sample ID	Core length (mm)	Angle (Rock-concrete)	$f_{t,\,b}$ (MPa)
1	205	75°	-
2	170	82°	-
3	100	84°	-
4	185	80°	-*
5	150	90°	-
6	240	67°	-

* Came loose when fixing the tool. All other core came loose while drilling.

Table 4-6. Measured gap between rock and concrete. Only for cores with bond. Core I02 is incorrectly reported as core "centrum" in Kalinowski (2018).

Drill core A03						
Distance from downstream surface (mm)	450	1 100	1 450	1 600	2 200	2 550
Gap width (mm)	0.3	0.7	0.4	0.6	0.4	0.4
Drill core B03						
Distance from downstream surface (mm)	10	450	1 200	1 650	1 900	
Gap width (mm)	0.4	0.3	0.2	0.4	0.6	
Drill core I02						
Distance from downstream surface (mm)	450	910	1 350	1 850		
Gap width (mm)	0.4	0.6	0.5	0.4		

4.1.4 Density

The average density of all tested samples from the plug is 2 253 kg/m^3 with a standard deviation of 118 kg/m^3. The individual results can be found in Kalinowski (2018). The average is higher than reported in Magnusson and Mathern (2015) for cube samples from plug production but almost identical to samples from the monolith cast next to the plug. The standard deviation is relatively high, but similar observations have been made when comparing production results and laboratory studies.

The stipulated value for calculations is 2 336 kg/m^3. The deviation results most likely from the higher air content of the mixes used for the production of the plug, see Grahm et al. (2015) for details. The increased air content of the concrete in the plug can explain certain observations such as lower average compressive strength than earlier laboratory tests.

4.1.5 E-modulus

The results in Table 4-7 are taken from Kalinowski (2018). The spread of the results is relatively large for cores 3-4 and 3-5, both within each core and in between the different cores. There is a certain amount of correlation to suggest that the outer part of the cores have a lower E-modulus compared the central parts. The value for 3-4 E1 is remarkably low but irregularities are not reported in the test report. However, when excluding the result for sample 3-4 E1, the spread of the whole test population is reduced significantly. The value of E_c is then in average 35 GPa which is very close the stipulated value of 34 GPa for calculations (Vogt et al. 2009). The results reported in Magnusson and Mathern (2015) are somewhat lower (31 GPa and 32 GPa) but comparable, taking into consideration that they were cured for one year.

Table 4-7. E-modulus of drill cores. In the two columns to the right, sample 3-4 E1 is excluded from the evaluation.

Sample ID	Level (mm)	E_0 (GPa)	E_c (GPa)	*E_0 (GPa)*	E_c (GPa)
3-4, E1	160–350	12.3	24.4	-	-
3-4, E2	800–900	30.1	36	*30.1*	*36*
3-4, E3	1 360–1 550	27.9	33.1	*27.9*	*33.1*
Avg. core 3-4		23.4	31.2	*29*	*34.55*
3-5, E1	250–440	29.5	36.2	*29.5*	*36.2*
3-5, E2	780–970	35.3	41	*35.3*	*41*
3-5, E3	1 620–1 810	25.4	29.7	*25.4*	*29.7*
Avg. core 3-5		30.1	35.6	*30.1*	*35.6*
3-6, E1	250–440	30.9	36.3	*30.9*	*36.3*
3-6, E2	800–900	29.7	35.5	*29.7*	*35.5*
3-6, E3	1 430–1 600	28.4	35.7	*28.4*	*35.7*
Avg. core 3-6		29.7	35.8	*29.7*	*35.8*
Avg, total		**27.7**	**34.2**	**29.7**	**35.4**
σ		**6.0**	**4.46**	**2.65**	**2.98**

4.1.6 Permeability

The results presented in Table 4-8 are taken from Kalinowski (2018). The average value is 38 mm water penetration and 2.24E–12 m/s permeability coefficient. The test results show a large spread, within the different cores as well as within each core. The corresponding value for laboratory samples from Vogt et al. (2009) is 5 mm and 3.86E–14 respectively. All test results from the plug are 3 to 15 times higher than the value determined on undisturbed laboratory samples. There were certain differences between the laboratory mixes and the mixes for the full-scale plug, namely a higher air content in the plug concrete. The influence of deviations in the mix design between plug concrete and laboratory concrete cannot be evaluated. It seems that the long-lasting water pressure, quick unloading for gas-tightness test and final stress test may have had a negative influence on the microstructure and thus the water tightness of the low-pH concrete. The highest levels of water penetration

are determined for samples situated closest to the downstream surface in the middle and upper parts of the plug. This generally corresponds to the observed frequency of microcracks in the concrete, see Section 4.2.3. Also, the simulated stresses were highest close to the downstream surface in the upper parts of the plug (see Grahm et al. 2015).

According to recent simulations in the KBP1016 project, the unloading prior to gas permeability test, will result in high tensile stresses. However, the concrete is still about 5 times denser than the stipulated design value of 1E–11.

Table 4-8. Water penetration by pressure test according to SS-EN 12390-8 and calculated permeability.

Sample ID	Water penetration (mm)	Calculated permeability (m/s)
3-1, 50–180 mm	44	2.99E–12
3-1, 990–1 130 mm	66	6.72E–12
3-1, 1 530–1 680 mm	44	2.99E–12
Average core 3-1	51	4.07E–12
3-2, 10–170 mm	73	8.22E–12
3-2, 1 000–1 150 mm	17	4.46E–13
3-2, 1 380– 1 530 mm	28	1.21E–12
Average core 3-2	39	2.39E–12
3-3, 50–160 mm	41	2.59E–12
3-3, 660–800 mm	14	3.02E–13
3-3, 1 430–1 550 mm	16	3.95E–13
Average core 3-3	24	8.64E–13
Average, total	**38**	**2.24E–12**

4.2 Other material properties

4.2.1 pH by leaching

Samples with a height of 12 mm and a diameter of 30 mm were extracted from drill cores. The position and ID of the samples is indicated in Table 4-9. The samples were submerged in beakers with approximately 30 ml of artificial saline water. The amount of water was adjusted to result in a rate of 0.85 between sample surface in cm^2 and water amount in ml. The pH was measured with a glass electrode and the water was partly exchanged according to the method description. All samples were stored in a glove-box with nitrogen atmosphere to avoid carbonation and thus falsification of the results.

Table 4-9. Samples for determination of pH. Level indicates the distance from the downstream surface. From Fjällberg (2018).

Sample ID	Level (mm)
3.1.1-1	0–300
3.1.1-2	940–970
3.1.1-3	1 880–1 920
3.2.1-1	0–300
3.2.1-2	870–900
3.2.1-3	1 750–1 780
3.3.1-1	0–30
3.3.1-2	890–920
3.3.1-3	1 740–1 770

The pH values increase initially during the first two weeks, due to leaching of alkalis. After about one month, the pH values stabilize. Equilibrium is reached after approximately 2 months. The recorded pH is between 9 and 9.5, see Figure 4-1. A lower value may be due to higher content of aggregates and thus less leachable paste in the individual sample. The results are consistent with measurements done within the low-pH project (KBP5001) on low-pH concrete B200 where an average pH of 9.5 was determined, using the same method.

All recorded pH values are well below the limit of pH = 11, stipulated in the post-closure safety concept for the repository.

4.2.2 Carbonation

The depth of carbonation was determined on freshly broken surfaces of drill core pieces with pH-indicator (phenolphthalein), see Kalinowski (2018) for details. For drill core, 3-4, the pH-indicator changed color at a depth of 7–16 mm from the surface. For drill core 3-6, the color changed at a depth of 7–17 mm. For the majority of the samples, the depth of color change is 7–9 mm. Note that for low-pH concrete, the indication of carbonation by use of pH indicator is somewhat difficult since the pH-difference between carbonated and uncarbonated concrete is much lower than in ordinary concrete.

Analysis of the depth of carbonation on thin sections is more exact. This analysis was done for three cores, 3-1.1, 3-2.1 and 3-3.1. These cores were taken from different heights in the plug, see Section 2.1. The analysis of the thin sections showed that the low-pH concrete was carbonated to a depth of 4.5–7.5 mm, see also Section 4.2.3 and Kalinowski (2018). This is a rather high carbonation depth for a highly humid environment and 5 years of exposure. At the same time, the carbonated layer had a much higher capillary porosity than the low-pH concrete deeper inside. There are two possibilities, either the carbonation resulted in a layer with high porosity, or, the higher porosity of the surface layer allowed for faster carbonation. A more detailed discussion of this phenomenon is found in the next section.

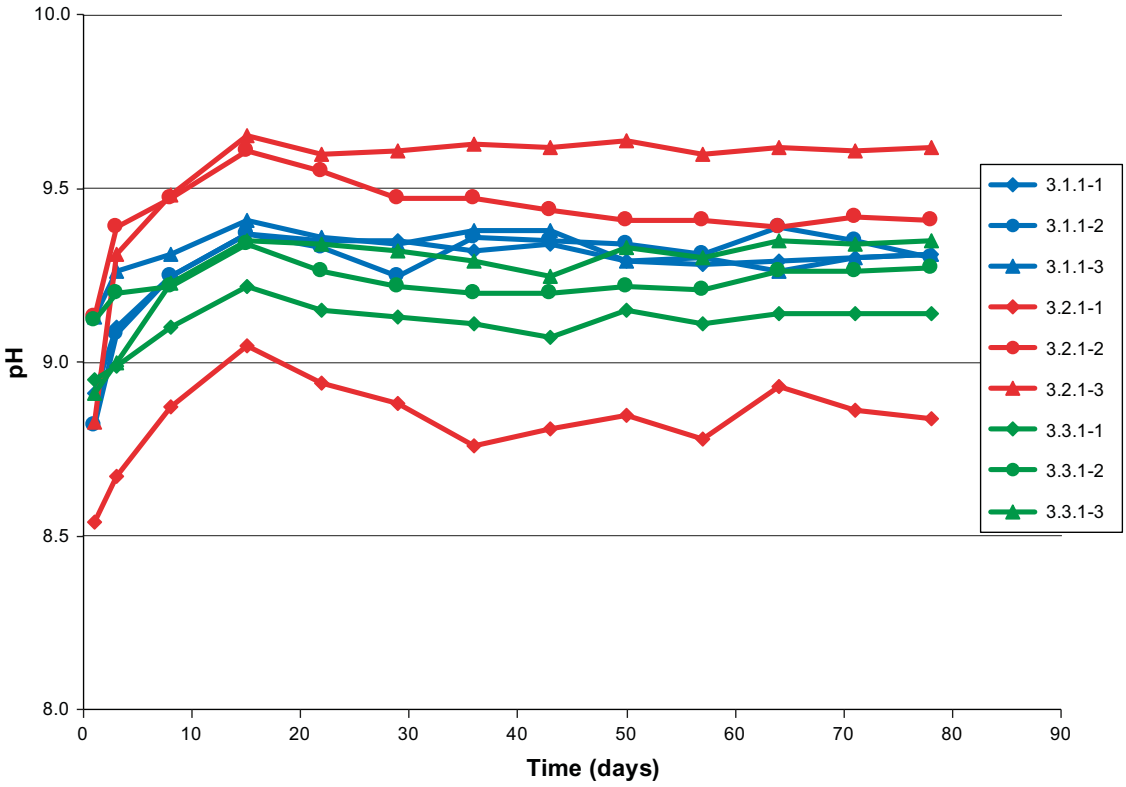

Figure 4-1. *Result of pH measurements. From Fjällberg (2018).*

4.2.3 Microstructure

The microstructure of the low-pH concrete from the drill cores was investigated primarily on thin sections. The samples were taken from "planned" cores at three different levels from the downstream surface, see Table 4-10.

Table 4-10. Samples for investigation of the microstructure in thin sections. Level indicates the distance from the downstream surface. From Kalinowski (2018).

Sample ID	Level (mm)
3.1.1-I	0–45
3.1.1-II	950–990
3.1.1-III	1 880–1 920
3.2.1-I	0–45
3.2.1-II	980–1 020
3.2.1-III	1 720–1 760
3.3.1-I	0–45
3.3.1-II	900–940
3.3.1-III	1 740–1 780

Table 4-11. Analysis of the microstructure of drill core 3.1.1 in thin sections. Level indicates the distance from the downstream surface. From Kalinowski (2018). For criteria, see Table 4-14.

Sample ID	3.1.1-I	3.1.1-II	3.1.1-III
Level	0–45 mm	950–990 mm	1 880–1 920 mm
Compaction of the concrete	Good	Good	Good
Homogenity of the cement paste	The surface of the concrete has a relativly high porosity*, elsewhere good	Good	Good
Equivalent w/c	0.45–0.50	< 0.35	< 0.35
Frequency of microcracks	High	High	Low
Miximum crack witdh in the thin section	0.01 mm	< 0.01 mm	< 0.01 mm
Depth of carbonation	5–7.5 mm		

* In the outer layer of the concrete to a depth of maximum 7.5 mm, a significantly higher capillary porosity was observed than at deeper depths in the concrete. This phenomenon is described in more detail below.

Table 4-12. Analysis of the microstructure of drill core 3.2.1 in thin sections. Level indicates the distance from the downstream surface. From Kalinowski (2018). For criteria, see Table 4-14.

Sample ID	3.2.1-I	3.2.1-II	3.2.1-III
Level	0–45 mm	980–1 020 mm	1 720–1 760 mm
Compaction of the concrete	Good	Good	Good
Homogenity of the cement paste	The surface of the concrete has a relativly high porosity*, elsewhere good	Good	Good
Equivalent w/c	0.45–0.50	< 0.35	< 0.35
Frequency of microcracks	Moderate	Low	Low
Miximum crack witdh in the thin section	0.05 mm	< 0.01 mm	< 0.01 mm
Depth of carbonation	4–7.5 mm		

* In the outer layer of the concrete to a depth of maximum 7.5 mm, a significantly higher capillary porosity was observed than at deeper depths in the concrete. This phenomenon is described in more detail below.

Table 4-13. Analysis of the microstructure of drill core 3.3.1 in thin sections. Level indicates the distance from the downstream surface. From Kalinowski (2018). For criteria, see Table 4-14.

Sample ID	3.3.1-I	3.3.1-II	3.3.1-III
Level	0–45 mm	900–940 mm	1 740–1 780 mm
Compaction of the concrete	Good	Good	Good
Homogenity of the cement paste	The surface of the concrete has a relativly high porosity*, elsewhere good	Good	Good
Equivalent w/c	0.45–0.50	< 0.35	< 0.35
Frequency of microcracks	Low	Low	Low
Miximum crack witdh in the thin section	< 0.01 mm	< 0.01 mm	< 0.01 mm
Depth of carbonation	6–7.5 mm		

* In the outer layer of the concrete to a depth of maximum 7.5 mm, a significantly higher capillary porosity was observed than at deeper depths in the concrete. This phenomenon is described in more detail below.

Criteria for the evaluation of the microstructure are summarized in Table 4-14. Guidance on the analysis of the microstructure of concrete in general and the evaluation of thin sections can be found in the literature, e.g. VTRC (2006).

In Figure 4-2 to Figure 4-4, examples of images from thin sections in UV-light and polarized light are shown. The observations are used for the evaluation in Table 4-11 to Table 4-13. The differences between porous surface layer and denser concrete below are clearly visible.

Table 4-14. Criteria for the evaluation of the microstructure in thin sections.

Criteria	Characterized by
Bad compaction	Concrete structure with agglomeration of air, air pockets around aggregate grains or reinforcement or entrapped air voids.
Good compaction	None of the above.
Bad homogenity	Uneven distribution of the binder components, including additives, in the concrete. An example of poor homogeneity is the separation of cement and water, which means that different areas of the concrete have different w/c. Strong microseparation of cement and water, which results in a network of areas with high capillary porosity in the concrete, is referred to as poor homogeneity.
Good homogenity	Even distribution of the binder components through the concrete mass. A certain microseparation is common in concrete. If the degree or extent of microseparation is considered to have no or insignificant effect on the properties of the concrete, homogeneity is referred to as good.
Low frequency of microcracks	Single isolated cracks. Low microcrack frequency probably does not have a significant impact on the concrete's properties.
High frequency of microcracks	A network of micro cracks. High microcrack frequency is likely to have a negative impact on the concrete's durability.

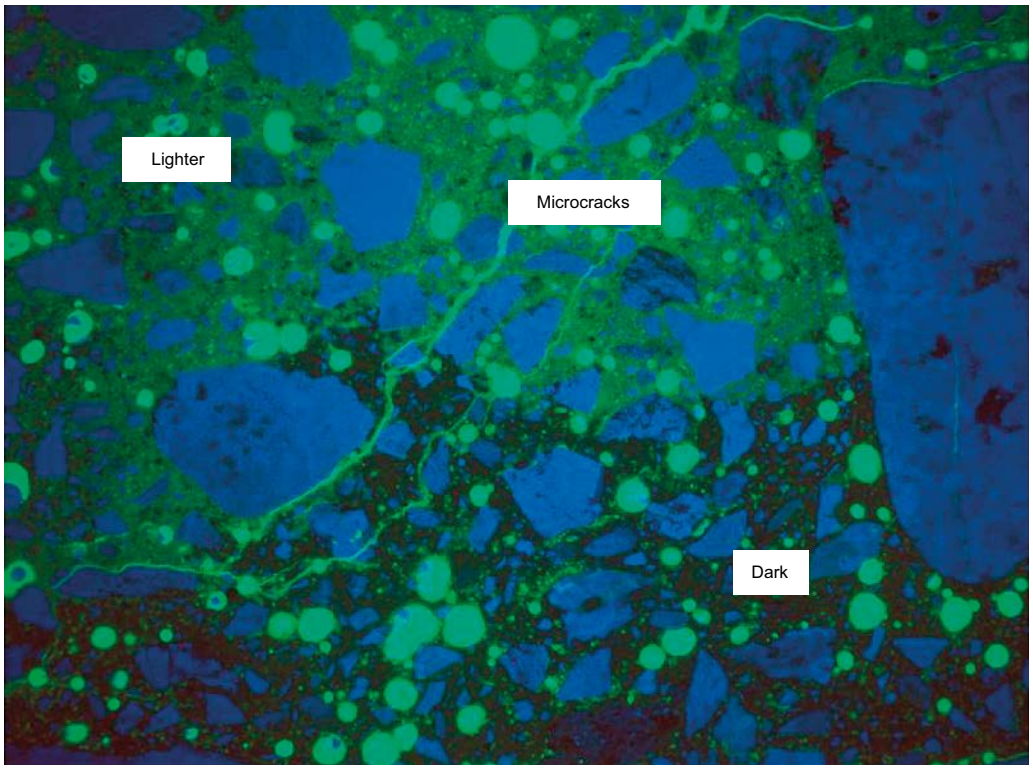

Figure 4-2. *Sample 3.2.1-I, 5–10 mm from the surface. UV-light. Width 6.7 mm. The difference between the porous surface (lighter color at the top) and denser concrete below is clearly visible. A microcrack runs from the surface inside the concrete. From Kalinowski (2018).*

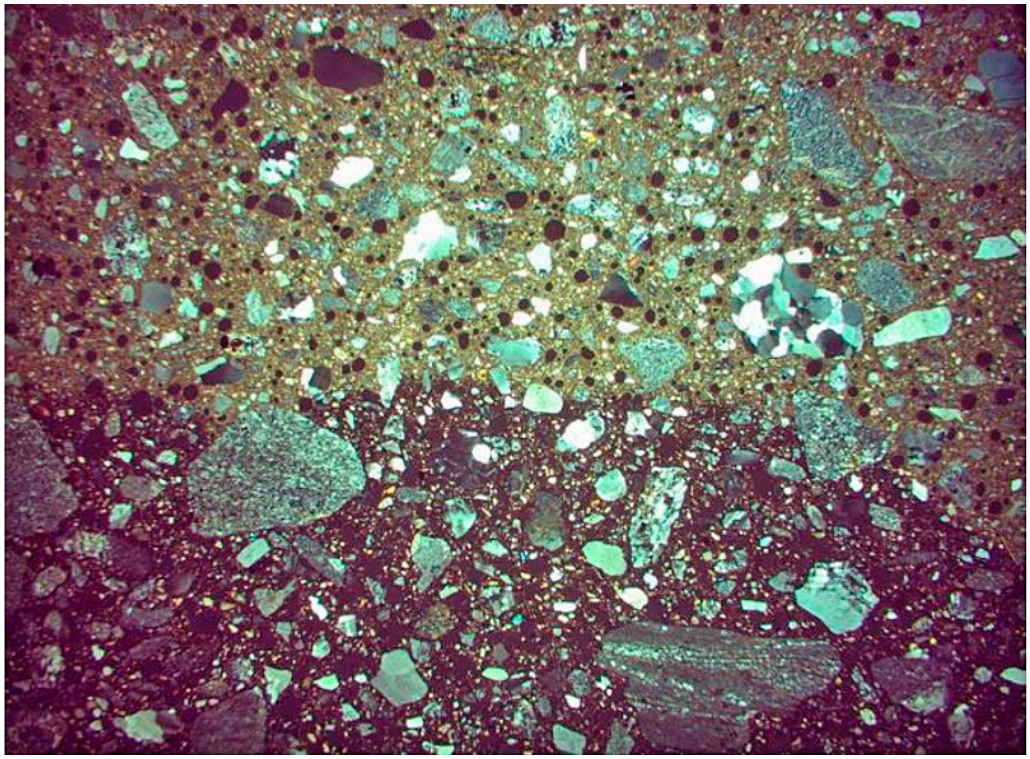

Figure 4-3. *Sample 3.1.1-I, downstream surface and inwards. Polarized light. Width 13.5 mm. The difference between the porous surface (lighter color at the top) and denser concrete below is clearly visible. The border marks even the depth of carbonation. From Kalinowski (2018).*

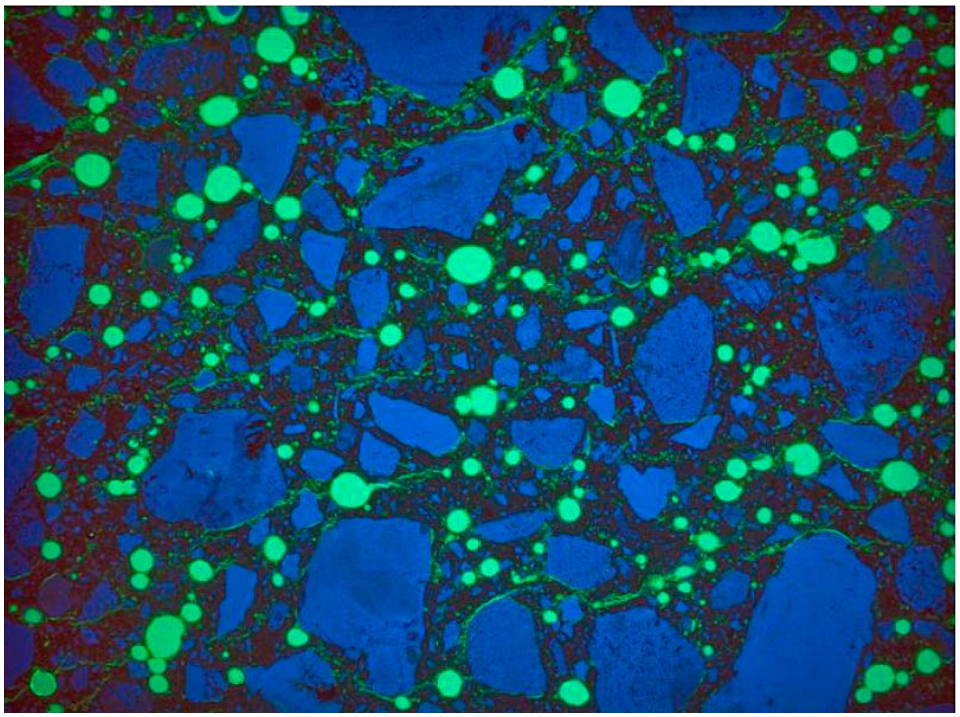

Figure 4-4. *Sample 3.2.1-II, 980 mm from the surface. UV-light. Width 6.7 mm. A system of microcracks in dense paste. From Kalinowski (2018).*

Table 4-15. Chemical composition of the cement paste in wt.%, average of at least 10 single analysis per depth. Areas of 0.1 × 0.1 mm analyzed. Compilation from Kalinowski (2018).

Sample ID	**p3-2 III**	**p3-4 nr1**	**p3-4 nr1**	**p3-4 nr1**	**p3-4 nr1**	**p3-4 nr1**	**p3-4 nr1**	**p3-4 nr1**	**p3-4 nr1**	**p3-4**
Depth (mm)	**Centr.**	**0.2**	**0.6**	**1.5**	**3**	**5**	**7**	**25**	**40**	**1 420**
Na_2O	0.1	0.3	0.3	0.3	0.4	0.4	0.3	0.3	0.2	0.3
MgO	1.6	1.4	1.1	1.0	1.1	1.1	1.2	1.6	1.5	1.5
Al_2O_3	2.5	3.2	2.3	2.7	2.4	2.8	2.2	2.8	2.8	3.0
SiO_2	32.5	32.8	32.5	31.7	33.4	32.9	32.7	33.6	32.9	33.8
SO_3	0.8	0.6	0.5	0.6	0.7	0.8	0.9	0.8	0.8	0.8
ClO	0.0	1.8	1.6	1.5	1.1	0.6	0.5	0.8	0.1	0.0
K_2O	0.5	0.6	0.5	0.6	0.5	0.5	0.5	0.6	0.7	0.6
CaO	58.8	55.7	58.5	58.5	57.8	58.6	59.3	56.2	57.6	56.8
TiO_2	0.2	0.3	0.1	0.2	0.1	0.1	0.1	0.1	0.1	0.1
Fe_2O_3	3.0	3.3	2.4	2.9	2.4	2.2	2.3	3.1	3.3	3.1
Total	100	100	100	100	100	100	100	100	100	100
CaO/SiO_2	1.8	1.7	1.8	1.8	1.7	1.8	1.8	1.7	1.8	1.7
Sample ID	**p3-6 nr 1**	**p3-6 nr 1**	**p3-6 nr 1**	**p3-6 nr 1**	**p3-6 nr 1**	**p3-6 nr 1**	**p3-6 nr 1**	**p3-6 nr 1**	**p3-6 nr 1**	**p3-6 nr4**
Depth (mm)	**0.2**	**1**	**2**	**4**	**6**	**8**	**10**	**12**	**18**	**1 600**
Na_2O	0.1	0.2	0.2	0.2	0.2	0.2	0.2	0.2	0.2	0.3
MgO	1.5	1.2	1.3	1.4	1.7	1.6	2.0	1.6	1.5	1.8
Al_2O_3	2.3	2.5	2.7	2.6	2.4	2.8	2.6	2.6	2.5	3.0
SiO_2	33.2	33.8	33.2	33.3	32.6	34.7	35.2	33.8	33.1	35.5
SO_3	0.8	0.8	0.8	0.9	0.8	0.9	0.9	0.9	0.9	0.8
ClO	0.7	1.2	1.4	1.0	1.7	0.4	0.1	0.0	0.0	0.0
K_2O	0.5	0.5	0.6	0.5	0.5	0.7	0.5	0.7	0.5	0.4
CaO	58.0	56.8	56.9	57.2	57.0	55.5	55.3	57.2	58.3	55.2
TiO_2	0.1	0.1	0.1	0.1	0.1	0.1	0.2	0.2	0.1	0.1
Fe_2O_3	2.8	2.8	2.8	2.8	2.9	3.0	3.0	2.9	2.9	2.9
Total	100	100	100	100	100	100	100	100	100	100
CaO/SiO_2	1.7	1.7	1.7	1.7	1.8	1.6	1.6	1.7	1.8	1.6

Table 4-16. Chemical composition of the cement paste in wt.%, average of at least 10 single analysis per depth. Point analysis, diameter 6 nm. Compilation from Kalinowski (2018).

Sample ID	3-4	3-4	3-4	3-4	3-4	3-4	3-4
Depth (mm)	0.05	0.1	0.5	1	2	15	1420
Na_2O	0.2	0.2	0.1	0.1	0.2	0.4	0.1
MgO	1.5	1.2	0.9	0.8	0.7	1.2	1.3
Al_2O_3	2.9	2.0	2.2	2.8	2.1	2.1	2.3
SiO_2	42.5	39.0	40.0	41.2	41.4	39.2	40.8
SO_3	0.6	0.6	0.8	0.7	0.5	0.9	1.0
ClO	1.6	1.2	1.5	1.5	1.3	1.8	0.0
K_2O	0.7	0.3	0.6	0.6	0.4	0.3	0.4
CaO	47.1	53.7	51.3	49.1	50.8	51.8	51.1
TiO_2	0.1	0.1	0.1	0.2	0.1	0.1	0.2
Fe_2O_3	2.9	1.8	2.7	2.9	2.5	2.1	2.8
Total	100	100	100.0	100.0	100	100.0	100
CaO/SiO_2	1.1	1.4	1.3	1.2	1.2	1.3	1.3
Sample ID	**3-6**	**3-6**	**3-6**	**3-6**	**3-6**	**3-6**	**3-6**
Depth (mm)	0.05	0.5	1	2	5	12	13
Na_2O	0.3	0.1	0.1	0.1	0.2	0.1	0.1
MgO	1.1	1.3	1.1	1.6	0.9	1.1	0.9
Al_2O_3	3.2	2.6	1.9	2.4	3.2	2.0	2.0
SiO_2	40.1	41.1	40.3	39.6	35.7	37.3	38.4
SO_3	0.8	1.2	0.8	0.9	0.8	0.9	0.9
ClO	1.0	1.3	1.0	1.1	0.8	0.3	0.0
K_2O	0.6	0.4	0.4	0.4	0.8	0.2	0.5
CaO	50.3	49.0	52.4	51.8	55.1	55.5	54.0
TiO_2	0.2	0.2	0.2	0.1	0.1	0.1	0.2
Fe_2O_3	2.6	2.9	2.0	2.1	2.4	2.5	2.8
Total	100.0	100	100	100	100.0	100.0	100
CaO/SiO_2	1.3	1.2	1.3	1.3	1.5	1.5	1.4

Below, certain properties of the low-pH concrete, observed in the thin sections, are analyzed and briefly discussed. The text is in parts a direct translation of the corresponding sections in Kalinowski (2018).

Cracks in the concrete

Samples 3.1.1-I and 3.2.1-I showed microcracks from the surface to a depth of 5 to 8 mm. In several thin sections, systems of short microcracks with a width < 0.01 mm were observed. The crack systems had a length of up to 7 mm. Given the maximum width of the fractures of less than 0.01 mm, it is estimated that, in their present size, their negative impact on the concrete's durability is negligible over 100 years. Like the singular microcracks, the microcrack systems have a preference in their orientation more or less parallel to the concrete's vertical surface. This limits the potentially negative impact of microcracks on the concrete's durability when exposed to saline water flowing over the vertical surfaces of the dome plug.

The number of short microcracks (frequency of microcracks) was found to be highest in samples "3.1.1 (I)" and "3.1.1 (II)". Both these samples came from concrete taken from the top of the dome plug. A minimum amount of short microcracks were observed in thin sections made of concrete taken from the lower part of the dome plug (drill core marked "3.3.1"). This indicates that the intensity of microcracks increases upwards in the concrete plug. However, the deepest cracks were observed in thin section "3.2.1 (I)" i.e. the downstream surface of the concrete taken from the center of the plug. In this thin section, there were surface cracking with the maximum crack width observed in this investigation, i.e. 0.05 mm and partly microcrack systems with the maximum length of 7 mm. The latter are at depths of 10–12 mm and were observed in the concrete from the drill core marked "3.2.1". The corresponding images can be found in Kalinowski (2018).

Two types of microcracks were observed in the thin sections. One type, which make up the majority of microcracks, has crack widths of < 0.01 mm and lengths of up to 1 mm. There are areas in the concrete where the frequency of these cracks becomes so high that they form networks. Some surface cracks, oriented more or less perpendicular to the concrete surface, were observed. This type of microcrack has a width of up to 0.05 mm at the concrete surface and runs to a depth of several millimeters into the concrete. Both types of microcracks run around ballast grains, indicating low energy in the cracking process. The microcracks have probably been formed due to shrinkage of the cement paste. Based on observations made in thin sections, there is no evidence of reduced durability of the concrete.

Carbonation

The maximum carbonation depth observed in thin sections is 7.5 mm. The carbonation front coincides well with the depth of surface layers in the concrete which shows a relatively high capillary porosity. Carbonated surface layers are shown in Figures 25–27, Kalinowski (2018).

High porosity in the surface layer

Cement paste in the outer part of the concrete has a higher capillary porosity than at larger depths. The capillary porosity in the outer layer corresponds to the capillary porosity of standard concrete with w/c ratio of 0.45–0.50, made with Degerhamn Anläggningscement without additives or fillers. By comparison, the inner parts of the plug have a porosity corresponding to standard concrete with w/c ratio < 0.35.

A layer of increased capillary porosity can generally be indicative of leaching of the concrete, caused by e.g. flowing water on the concrete surface. In normal cases, leaching involves decomposition and loss of calcium oxide. No decrease in the amount of calcium oxide has been observed in areas with increased capillary porosity. CaO/SiO_2 ratios noted from the analysis of the chemical composition of the binder support this observation (see below). The gradient and depth of the porous layer appears to be the same for all three thin sections that were made of concrete taken from different parts of the dome plug. Such an equivalent leaching would mean an identical water exposure on the concrete in all three areas, which is highly unlikely.

An alternative explanation for the relatively high capillary porosity in the surface layer is that there was water in the formwork that got mixed into the concrete's outer part while casting. However, it should be noted that even if this was the case, the areas with increased capillary porosity would most likely have a different thickness in different areas of the concrete.

A third possible explanation is that the surface layer of the dome plug was not cured as well as the rest of the plug or that substances which were applied to the formwork hindered adequate hydration of the concrete's surface layer. According to information from people involved in the manufacturing of the formwork for the plug, the wooden formwork was coated with some kind of paint. Some types of paint contain substances which might hinder the hydration process of fresh concrete.

The carbonation front in the concrete's outer layer coincides with the area which exhibits relatively high capillary porosity. In standard Portland cement paste, carbonation reduces the capillary porosity. When the binder consists of Portland cement with a high content (40 %) of silica fume, there is no information available if this still applies. At the same time, there are no theoretical reasons that could explain increased capillary porosity in carbonated binder consisting of the said mixture. It is therefore likely that the relatively high capillary porosity has existed prior to carbonation and the carbonation front reflects the depth of cement paste with relatively high gas permeability.

An unpublished investigation on the carbonation of low-pH concrete showed that, as in traditional concrete, carbonation results in reduced porosity of the carbonated layer. The integrity of the low-pH concrete was found to be unharmed after carbonation. The rate of carbonation can be expected to be 10–20 % higher in low-pH concrete than in traditional concrete with similar strength for the same exposure. The recommended value for the prediction of carbonation of low-pH concrete in moist tunnel environment is 1.5–3 mm/$\sqrt{year}$. This gives a carbonation depth of 3.3–6.7 mm for the plug after 5 years. This roughly correlates with the observations on the samples taken from the dome plug. The observed increase in porosity close to the surface in the plug is not in accordance with these unpublished results.

Miscellaneous

The limestone filler appears to be evenly distributed throughout the concrete.

Chemical composition of the cement paste, analyzed in SEM

The chemical composition of the cement paste, analyzed on areas of 0.1 × 0.1 mm and spots, is summarized in Table 4-15 and Table 4-16. Averages of at least 10 individual analyses are presented. The individual analyses can be found in Kalinowski (2018).

Analyses of the composition of the binder at different depths in the concrete were made using EDS/SEM on concrete surfaces. Experience shows that analysis of fractured surfaces in cement paste provide a more representative chemical composition than analysis on ground/polished surfaces. The disadvantage of fractured surfaces is that the control of the analyzed areas with BSE detector, in order to avoid aggregate grains, is less certain. Control of fractured surfaces with the BSE detector also does not provide information about the amount of limestone filler in the area analyzed. Since the binder in low-pH concrete contains Portland cement, silica fume and limestone filler, analysis with the BSE detector has an obvious disadvantage.

The chemical composition of the cement paste was analyzed on areas with a size of 0.1 × 0.1 mm and on points. Analysis of areas 0.1 × 0.1 mm is thought to provide a good representation of the composition of the binder in general but at the same time, the analysis contains fractions of limestone filler. In the structural analysis of the concrete in thin sections, the limestone filler was found to be evenly distributed throughout the concrete. Therefore, it can be assumed that the fraction of limestone filler in the analytical results, which includes elevated calcium levels, is the same in the various analyzed areas in the concrete.

Point analyses involve analysis areas with a diameter of 6 nanometers. These analyses are expected to provide more significant values for cement paste's chemical composition since the disturbance by limestone filler can be assumed to be smaller. At the same time, point analyses represent a significantly smaller part of the cement paste compared with analysis of areas with a of size 0.1 × 0.1 mm. Point analysis irradiates the sample area with an electron beam of a small diameter. The analyzed area in the sample is much smaller but has a larger depth since the electron beam burns a pit in the sample. Thus, disturbances by limestone fillers cannot be completely avoided even with the use of spot analysis. However, these disturbances should be minor for this type of analysis.

Intrusion of substances from outside

There has been a penetration of chloride ions into the outer part of the concrete. In samples "3-4" chlorides have been detected to a depth of at least 40 mm into the concrete. At this depth, the chloride levels of 0.1 % by weight were noted, which is the minimum detection level of the method. In sample "3-6" a chloride content was observed to a depth of 10 mm in the concrete. At depths of 12 mm into the concrete, samples "3-6" showed that the levels were below the detection limit (i.e. < 0.1 % by weight). At depths of 1 420 mm in sample "3-4" and 850 mm in sample "3-2.1", the chloride content is below the detection limit of the method, i.e. there is no evidence of penetration of chloride ions into the concrete.

Contents of magnesium measured in the concrete's outer layer, at a depth of 0.2 mm in the concrete (samples "3-4" and "3-6") were slightly higher than contents measured at depths of 1–2 mm and 1–7 mm respectively. However, measured Mg levels at even greater depth in the concrete from these two samples were at the same level as in the outermost layers, i.e. 1.4–1.8 % by weight. Results from spot analyzes in samples "3-4" showed a little higher mean MgO at a depth of 0.05 mm in concrete compared with greater depth in the concrete.

No increase in sulphate content in the concrete's outer layer were observed in the analyses.

Leaching of the cement paste

The chemical composition of the cement paste was analyzed for different depths. The analysis was performed on areas of 0.1 × 0.1 mm. The results of this type of analysis (samples "3-2.1", "3-4" and "3-6") yielded CaO/SiO_2 ratio of 1.7 ± 0.1. The variation of the quota of ± 0.1 is estimated to be within the uncertainty of the analysis method for each individual EDS analysis.

CaO/SiO_2 ratios of the binder, calculated from normalized EDS results, indicate that there has been no leaching of calcium from the concrete in the analyzed samples "3-4" and "3-6".

The spot analysis for corresponding samples gives a CaO/SiO_2 ratio of 1.3 ± 0.1. Thus, the disturbing influence of limestone filler appears to be somewhat reduced when using spot analysis. Still the results would appear to indicate that the cement paste is not yet at equilibrium since the theoretical value for the CaO/SiO_2 ratio is approximately 0.75 (Vogt et al. 2009). The theoretical value for the CaO/SiO_2 ratio can be calculated from the content of CaO in the cement and the content of SiO_2 in the cement and the silica fume. In Vogt et al. (2009), values of 0.70 to 0.85 for the CaO/SiO_2 ratio of low pH concrete with identical composition were measured, using polished samples. It seems that polished samples simplify the avoidance of limestone filler in the analysis. Also, different operators may influence the results unintentionally.

4.2.4 Degree of capillary saturation

The calculated degree of capillary saturation is presented in Table 4-17. Almost all samples had a high degree of water saturation (> 90 %), i.e. the concrete in the plug contained high amounts of moisture. This is not unexpected since the plug is exposed to water pressure on one side and relatively high humidity on the other side. There is a weak tendency that suggests lower saturation values close to the downstream surface. A certain, unknown error is included in the presented results since the samples were extracted from the drill cores several days after the cores were drilled from the plug. This allows for redistribution of moisture and also drying. This could not be avoided due to logistical reasons. Ideally, samples are extracted and weighed immediately after drilling. Presumably is the degree of capillary saturation somewhat higher than measured on the actual samples. However, the error is inherently included in all the results. The samples required rather a long time to absorb and release moisture, see Figure 4-5. This indicates a very dense microstructure with low porosity.

Table 4-17. Degree of capillary saturation. Level indicates the position of the individual sample in the drill core. Positive values indicate distance from the downstream surface of a core. Negative values indicate the distance from the end of the drill core. Extracted from Andersson (2018).

Sample ID	Level (mm)	Position in the plug	Calculated degree of capillary saturation (-)
3-6:1	200	Top	0.94
3-1:2	900		0.90
3-6:4	–200		0.94
3-5:1	200	Center	0.93
3-2:2	910		0.95
3-2:3	–200		0.95
3-3:1	200	Bottom	0.88
3-3:3	920		0.95
3-3:4	–250		0.95

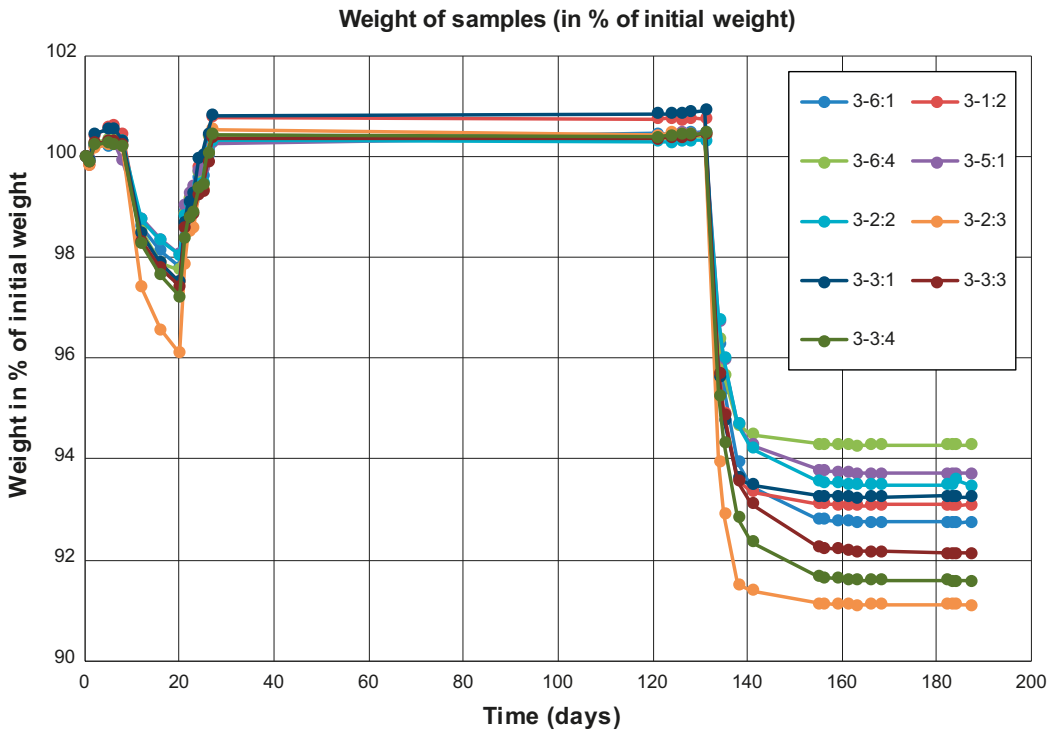

Figure 4-5. *Weight of samples vs time. The first drying cycle after 10 days is not normal procedure. It was performed since the absorption of moisture was extremely slow and thus, mistakes in method were assumed. This is deemed to have no influence on the final result.*

4.3 Conclusions

The visual inspection of the concrete drill cores revealed no obvious defects like cracks, honeycombing or insufficient embedment of cast-in items. For one core, a certain reduction in the content of coarse aggregate was observed. This may be due to a slight segregation of coarse aggregate caused either by a "sieving action" from cast-in items during the concrete pour, in the pump or in the concrete truck itself prior to the pour. The tested mechanical properties for this section of drill core do not differ significantly from other samples. Thus, the lower aggregate content has no obvious negative effect. Similar observations have been made for castings with normal self-compacting concrete.

The drill cores in the interface between rock and concrete show that the top part of the slot was not completely filled with concrete or grout. This defect originates from incomplete filling when casting the plug.

The interface between the concrete and the rock was, for all observed cores, filled with a certain amount of grout (though not downstream of the outer water stops). More grout was observed in the cores situated in the top and to the side of the dome plug. This can be expected and is due to the effects of shrinkage (autogenous, drying and thermal in combination with gravity).

A certain bond strength between rock/grout and concrete must exist since all drill cores through the interface did not fall apart immediately after drilling and removal from the holes. The actual bond strength between rock/grout and concrete could only be determined for one sample in the laboratory. For all other samples, the concrete came loose during transportation and sample preparation.

When tested in situ, no value for the bond strength between the concrete and the rock could be obtained either. One obvious reason is that the samples were situated too close to a grouting pipe with steel fixation and protective geotextile, thus breaking the bond. However, the overall view suggests that there is a certain bond strength between the concrete and the rock. The bond is inconsistent with partly low bond strength and partly no measurable strength at all.

Most of the mechanical properties investigated are, on average, comparable with undisturbed samples from earlier tests or from the monolith cast beside the plug. This indicates no dramatic decrease in the mechanical properties of the low-pH concrete due to aging, loading and restrained shrinkage. However, when analyzing the results in more detail, there are indications that the concrete may have been influenced negatively in certain areas. The compressive strength is lower close to the surfaces of the plug and the average tensile strength appears to be somewhat lower when compared with results from earlier tests. The permeability of the tested concrete samples is higher in the upper parts of the dome plug and close to the downstream surface. These observations coincide with results from investigations of the microstructure.

The investigations of the microstructure revealed more microcracks close to the surface of the plug. This may originate from loading or restrained shrinkage and correlates with certain results from tests on the mechanical properties (see above). The reason for the existence of a surface layer with increased porosity could not be exactly determined. The possibility that leaching or carbonation has caused this layer with high porosity is deemed unlikely. The most plausible explanation is that the high porosity in the surface layer was caused during pouring of the concrete or insufficient curing. The chemical analysis of the paste showed that chlorides penetrated unevenly from the downstream surface, the depth of penetration varies between 10 mm and 40 mm. The determined CaO/SiO_2 ratio is higher than values determined in Vogt et al. (2009) and also higher than the theoretical value of ca 0.75, presumably due to the incorporation of limestone filler in the analysis. The determined pH value by leaching tests is consistent with earlier investigations on laboratory samples. Thus, the composition of the C-S-H in the low-pH concrete from the plug should, in all probability, be similar to those found in laboratory samples.

The comparison of stipulated values for material properties for structural calculations from earlier laboratory tests with tested values shows that the concrete in the plug is consistent with most of the anticipated parameters with the exception of tensile strength. (see Table 4-18). It should be noted that the concrete was subjected to severe loading and quick unloading, as well as restrained shrinkage which may have resulted in microcracking. This was confirmed by investigations of the microstructure.

Table 4-18. Material parameters used for the design of the dome plug, from Grahm et al. (2015) and tested results.

Material parameter	Stipulated value	Test result	Remark
Compressive strength f_{ck} (90 d, cylinder)	54 MPa	50.3 MPa	OK acc. to SS-EN 13791, Maybe due to high air content
Tensile strength f_{ctk}	2.9 MPa	1.95 MPa	Maybe due to high air or microcracks
E-modulus E_{cm}	34 GPa	35 GPa	
Density	2336 kg/m^3	2253 kg/m^3	Due to high air content. Not a critical parameter
Other important properties			
Permeability coefficient K	10^{-11} m/s	2.24×10^{-12} m/s	Maybe due to high air or microcracks

4.3.1 Possible improvements

One of the most important observations made while investigating and dismantling the dome plug was that the top part of the slot was not filled with concrete. Since grouting was terminated before this void was filled with grout, a triangular void with a height of approximately 50 cm remained. It is impressive that the dome plug performed as expected, despite this defect. In future production, this type of defect shall be avoided.

There are several possible solutions to this problem. For the highest chance of success, a combination of several measures should be used.

- Install cameras, sensors or similar on top of the slot in order to ensure that pumping is not terminated before the slot is completely filled.
- Increase the number and diameter of venting pipes at the top of the slot. Observe that these pipes have to be removed when casting is finished since they may provide possible leakage passageways.
- Cast the top part of the plug (into the slot) with a modified concrete mix design. The amount of coarse aggregate could be reduced and the dosage of superplasticizer increased for enhanced flowability of the low-pH concrete. This should simplify complete filling of the slot.
- Place one or more extra pumping pipe(s) at the top of the slot. Observe that these pipes need to be removed when casting is finished since they may provide possible leakage passageways. Venting pipes are required.
- Drill one or more holes from the downstream side of the plug through the rock to the top of the slot. Cast the last part of the plug from the top of the slot. The drilled hole is to be filled with concrete once the plug is finished. Venting pipes are required.
- Allow for increased grouting in order to fill voids. This should be seen as a last resort instead of having to replace a faulty plug. Dismantling a faulty plug and constructing a new plug possibly also includes having to remove and replace the bentonite in the barrier.

5 Additional results from the low pH project

Results from long-term tests series are presented in this section. These long-term tests were initiated in the now terminated low-pH concrete project (KBP5001) but were hitherto not reported.

5.1 Compressive strength and splitting tensile strength of samples from the “monolith”

Tests on compressive strength and splitting tensile strength were conducted in 2015 and 2016. Samples were taken from the monolith cast next to the dome plug on 13th of march 2013. Table 5-1 summarizes the results, details can be found in Ikink (2015) and Olsson (2016).

The average compressive strength is 76 MPa, the spread in between the samples is small which is expected since the individual samples origin from only one drill core each. In Magnusson and Mathern (2015), 74 MPa are reported for 1-year old samples. There is almost no difference between the results after one year, two years and three years. Thus, the concrete in the monolith does not seem to gain or lose compressive strength after 1 year of curing.

The average splitting tensile strength is 6.4 MPa, the standard deviation is comparable to other test series, e.g. in Magnusson and Mathern (2015). The result for one-year old samples in Magnusson and Mathern (2015) is 6.3 MPa, to be compared with 6.5 MPa after two years and 6.2 MPa after 3 years of ardening. The splitting tensile strength seems to be more or less constant after 1 year.

Table 5-1. Compressive strength and splitting tensile strength. Test results from Ikink (2015) and Olsson (2016).

Sample ID	Age (days)	f_{cc} (MPa)	$f_{ct,\,sp}$ (MPa)
61-H-TK-150-747	747	72.1	
61-H-TK-450-747	747	77.6	
61-H-TK-750-747	747	79.2	
62-H-SK-150-747	747		6.3
62-H-SK-450-747	747		6.15
62-H-SK-750-747	747		7.1
Avg. 747 days		76.3	6.5
71-H-TK-150-1113	1 113	74.6	
71-H-TK-450-1113	1 113	75.4	
71-H-TK-750-1113	1 113	75.7	
72-H-SK-150-1113	1 113		6.2
72-H-SK-450-1113	1 113		5.9
72-H-SK-750-1113	1 113		6.45
Avg. 1 113 days		75.2	6.2
Avg. total		**75.8**	**6.4**
σ		**2.24**	**0.37**

5.2 Creep results

Creep tests were conducted on sealed concrete cylinders for three different stress levels, approximately 40 %, 50 % and 75 % of the compressive strength. The methodology, details and initial results until 2014 are presented in Flansbjer and Magnusson (2014). Initially, the test series was planned to be terminated after three years but was prolonged to 6 years. The final results after 6 years of loading are presented in Figure 5-1 to Figure 5-7.

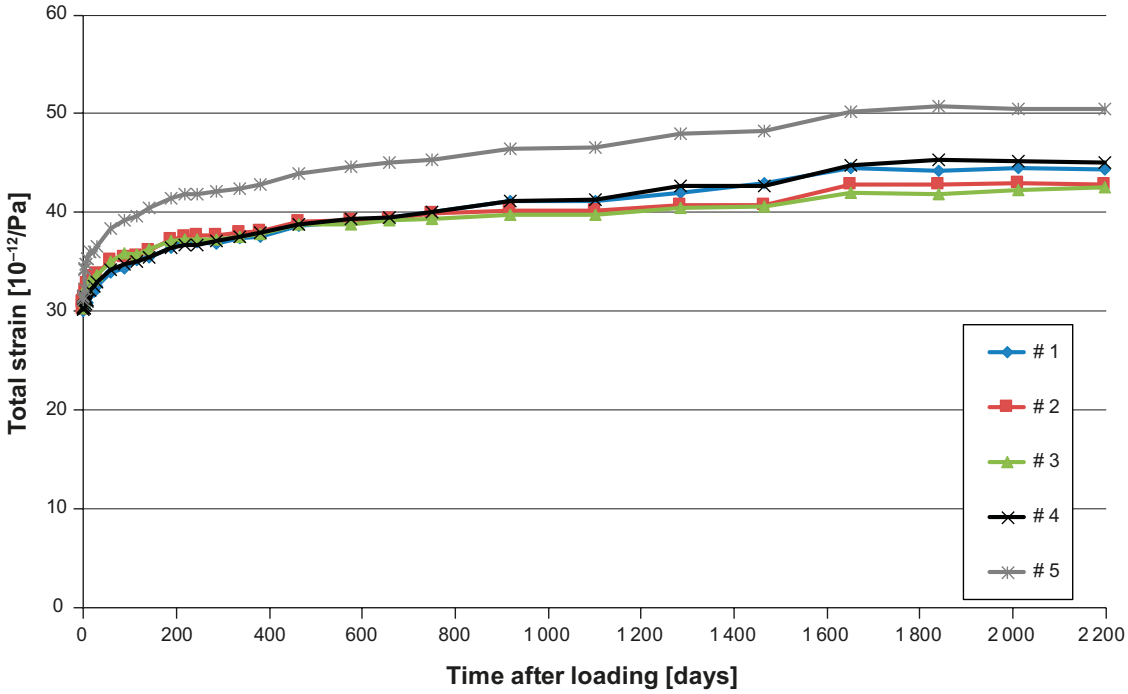

Figure 5-1. *Total stress-induced strain versus time after loading for the creep specimens of test run (TR) 1a; applied stress $\sigma_{cm}(t0)$ = 30.0 MPa (40 % f_{cc}).*

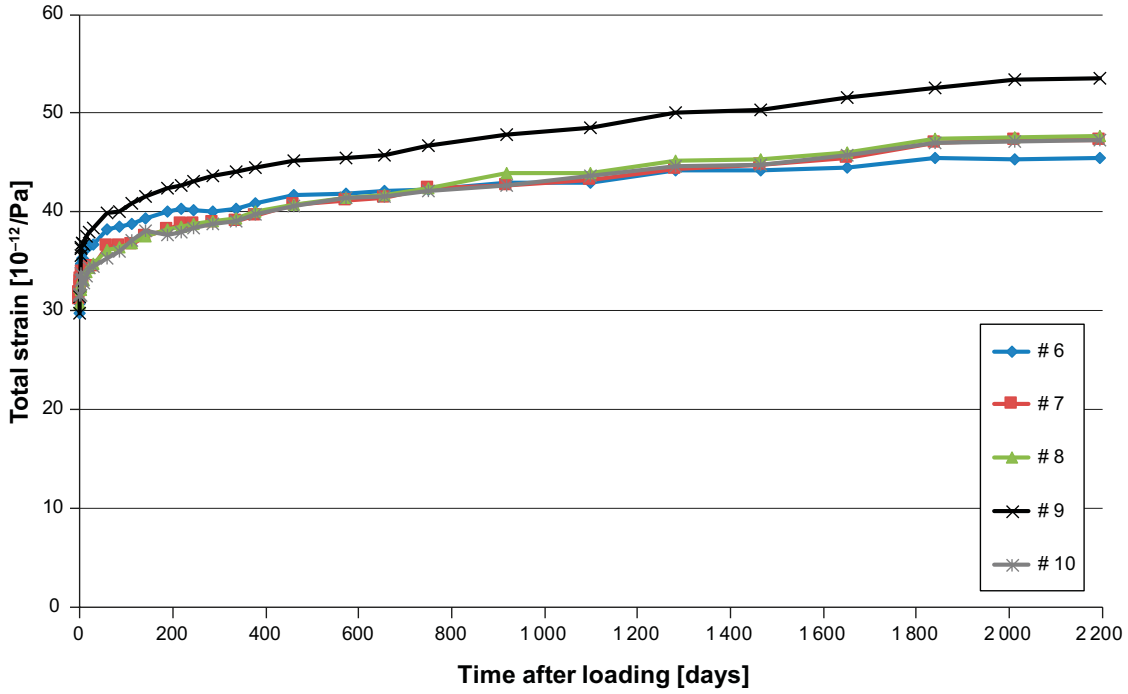

Figure 5-2. *Total stress-induced strain versus time after loading for the creep specimens of test run (TR) 1b; applied stress $\sigma_{cm}(t0)$ = 38.5 MPa (50 % f_{cc}).*

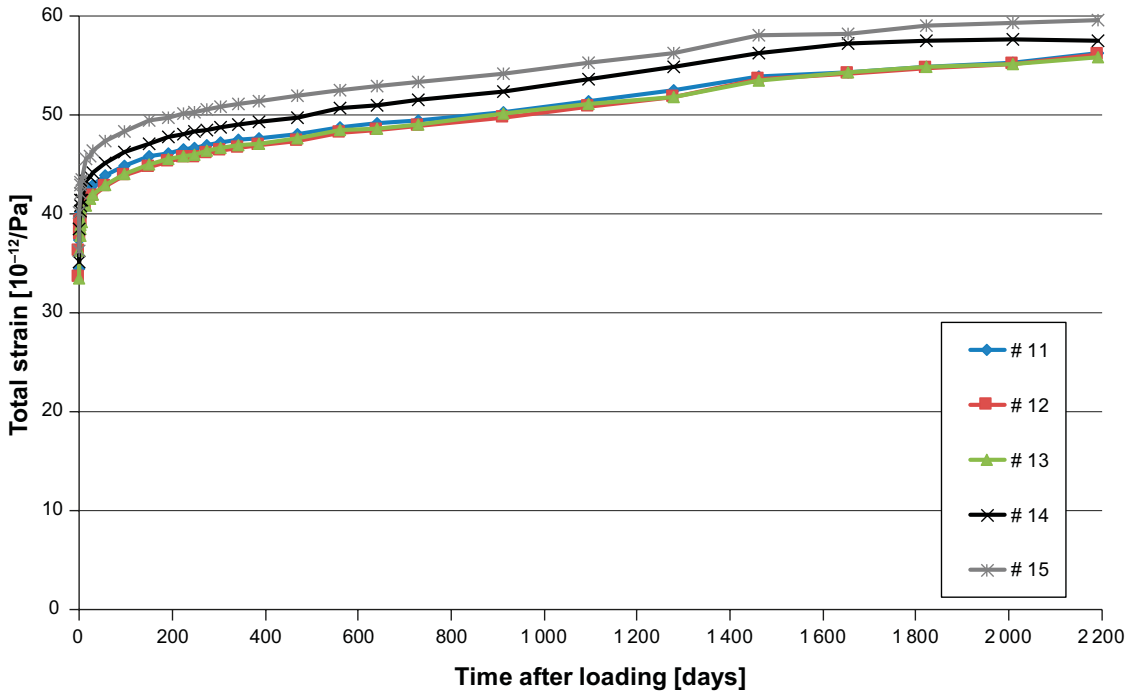

Figure 5-3. *Total stress-induced strain versus time after loading for the creep specimens of test run (TR) 2; applied stress $\sigma_{cm}(t0)$ = 49.4 MPa (75 % f_{cc}).*

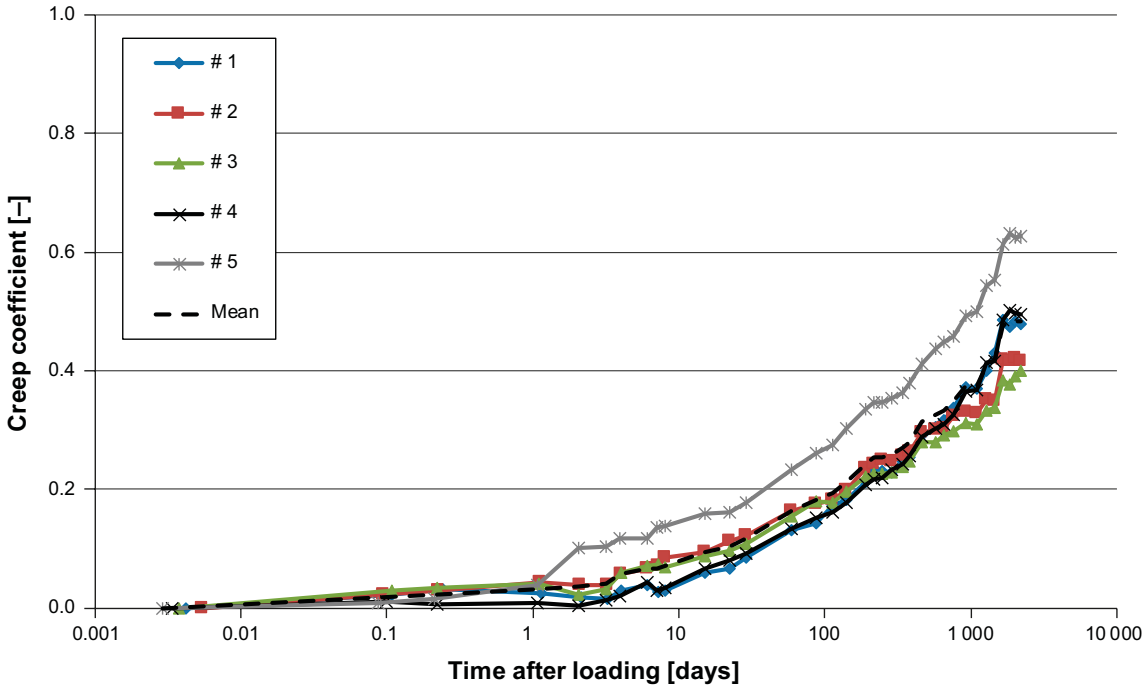

Figure 5-4. *Creep coefficient versus time after loading for the creep specimens of test run (TR) 1a; applied stress $\sigma_{cm}(t0)$ = 30.0 MPa (40 % f_{cc}).*

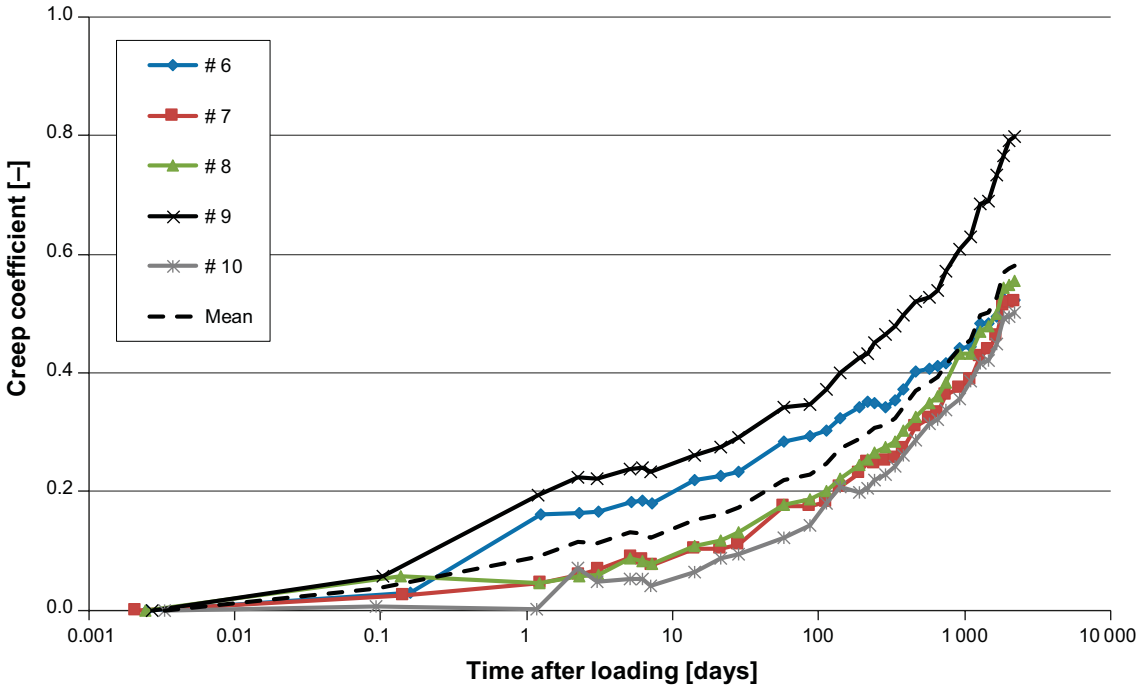

Figure 5-5. *Creep coefficient versus time after loading for the creep specimens of test run (TR) 1b; applied stress $\sigma_{cm}(t0)$ = 38.5 MPa (50 % f_{cc}).*

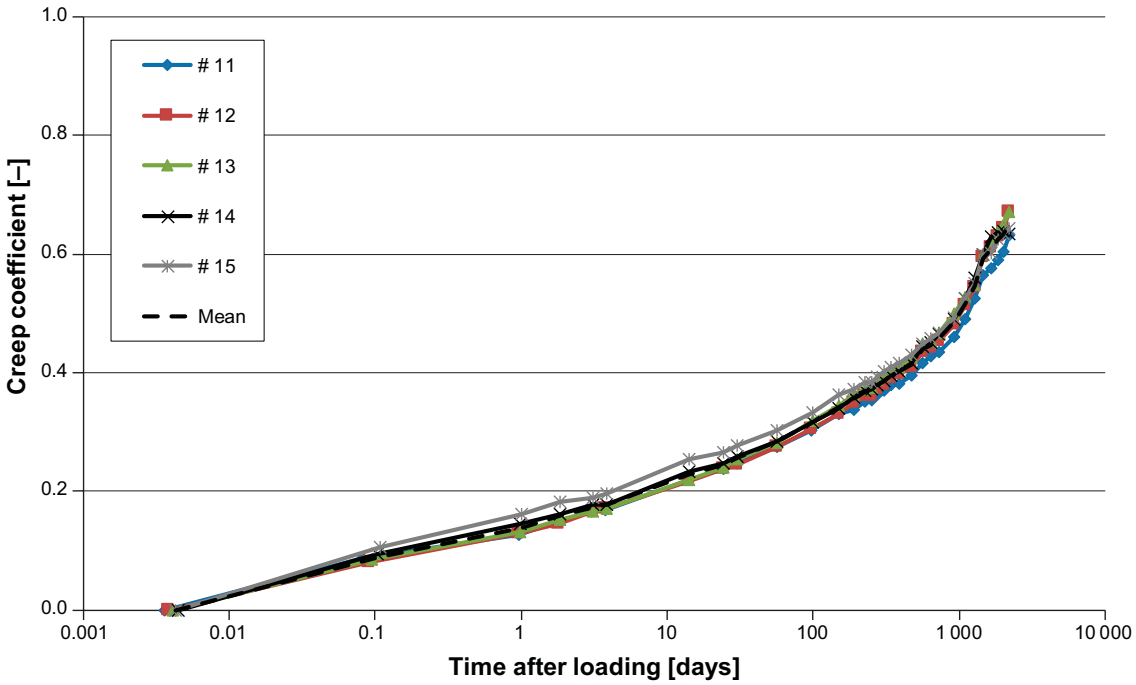

Figure 5-6. *Creep coefficient versus time after loading for the creep specimens of test run (TR) 2; applied stress $\sigma_{cm}(t0)$ = 49.4 MPa (75 % f_{cc}).*

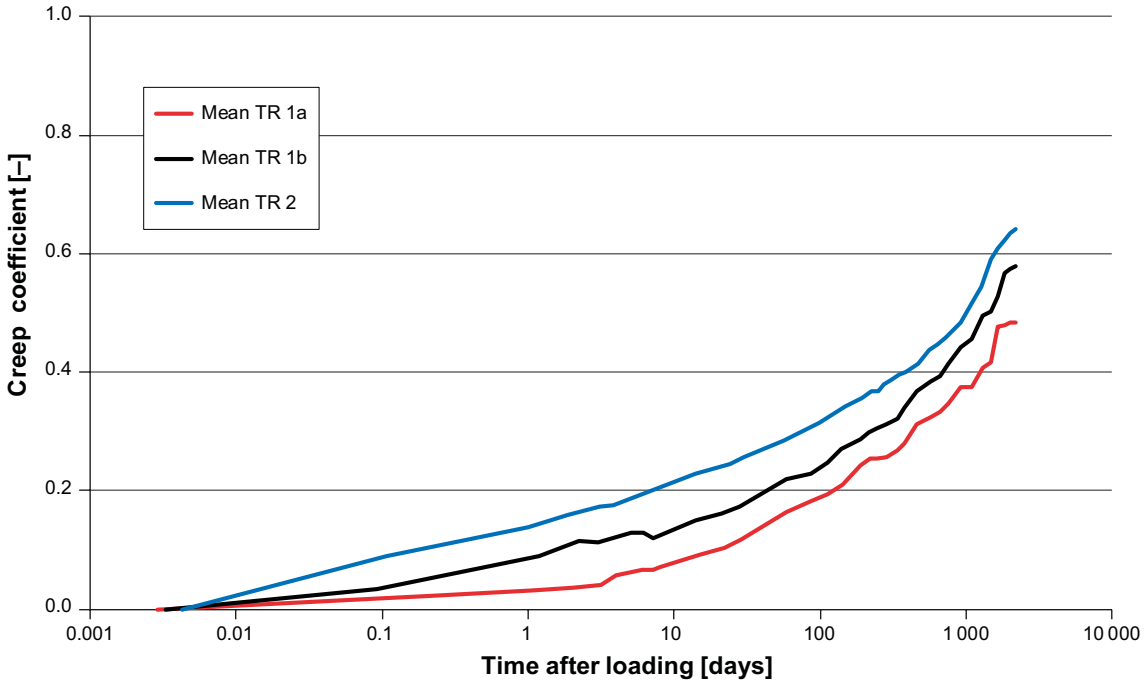

Figure 5-7. *Mean value of the creep coefficient versus time for TR 1a ($\sigma_{cm}(t0)$ = 30.0 MPa), TR 1b ($\sigma_{cm}(t0)$ = 38.5 MPa) and TR2 ($\sigma_{cm}(t0)$ = 49.4 MPa).*

The creep behavior of low-pH concrete at high stress levels was studied. Not unexpectedly, the higher stress levels result in higher creep deformations. The difference of the creep coefficient between the different stress levels is almost constant from day one after loading until the test was terminated. The values in Figure 5-7 correlate with earlier test, see Figure 5-8. The higher the stress level, the higher the creep coefficient. Observe that all samples had approximately the same age when loading started.

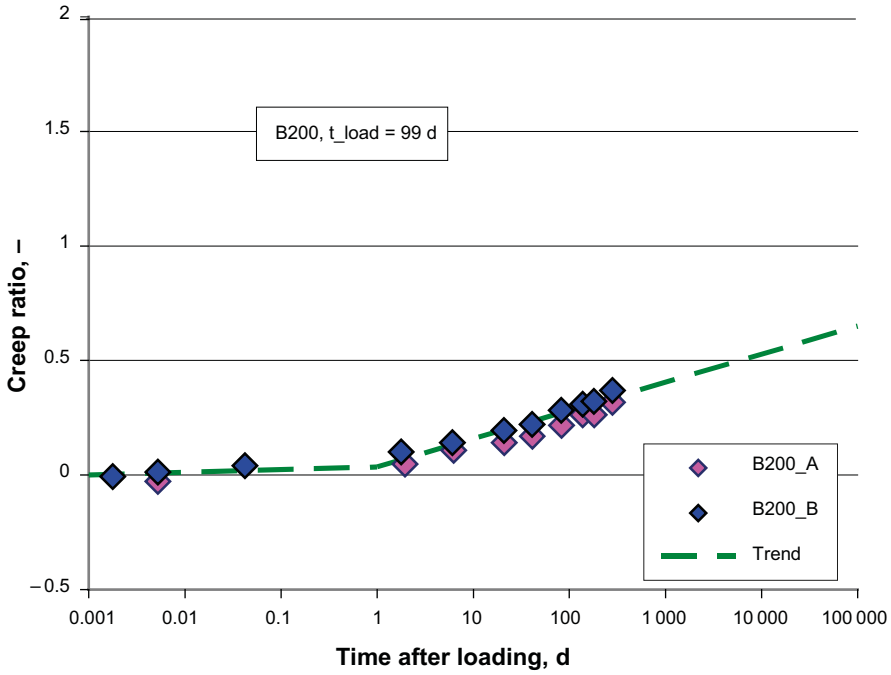

Figure 5-8. *Creep test with stress level of approximately 20 % of the compressive strength, from Vogt et al. (2009).*

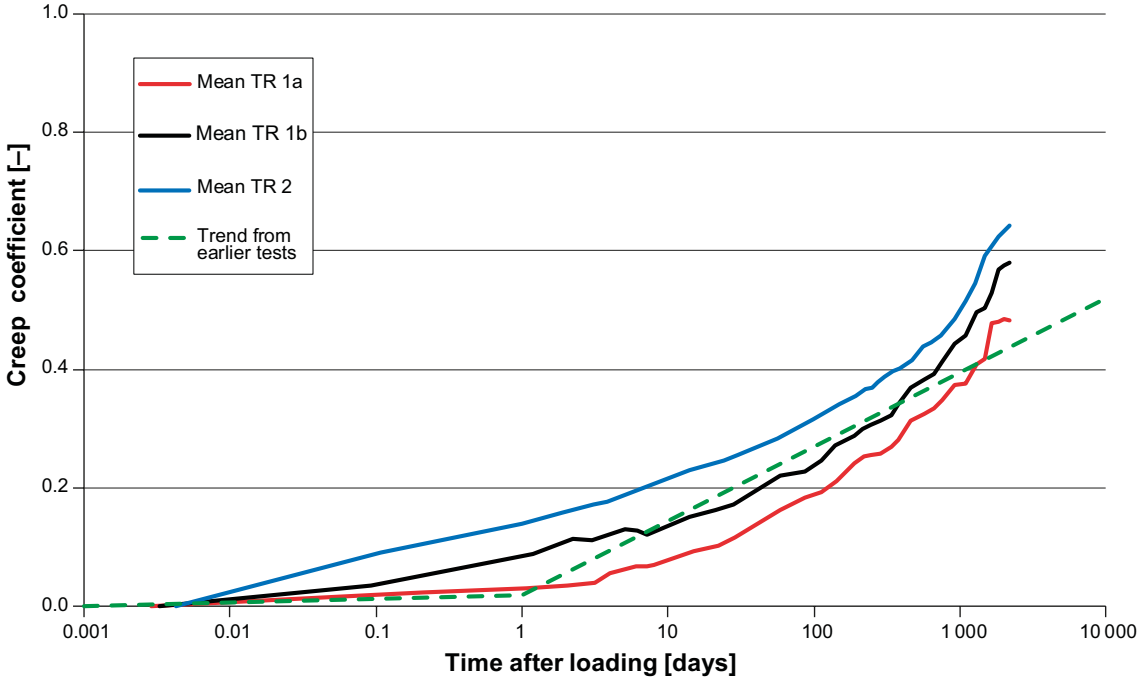

Figure 5-9. *Combination of Figure 5-7 and Figure 5-8.*

5.3 Compressive strength of creep samples

The compressive strength of the cylindrical samples used for the creep test (previous section) was determined in order to evaluate if 6 years of loading resulted in structural damage of the concrete and thus decreased compressive strength. Before the creep test, samples from series TR1 had a compressive strength of 70.5 MPa (cylinders ∅ 100 × 300 mm). The samples of series TR2 had a compressive strength of 67.8 MPa (cylinders ∅ 90 × 270 mm) before the creep test. One has to keep in mind that all samples were cured and stored in exactly the same conditions.

The results are displayed in Table 5-2. Series “Grupp 1, Ref 1–Ref 5” is excluded from the evaluation since the compressive strength was unexpectedly low and the spread of the results abnormally high. This was presumably due to insufficient quality of the sample preparation (grinding of the upper and lower surfaces) which did not influence the function of the individual samples as shrinkage references but had a large impact on compressive strength results.

Comparing the creep samples from series TR1a and TR1b with the corresponding references (extra samples TR1), the strength of the loaded specimens is almost 10 MPa higher than the strength of the references. The same can be noticed for series TR2, an increase in strength in the order of 10 MPa. That is an unexpected result. One would assume a certain reduction in compressive strength due to formation of microcracks during 6 years of exposure to high compressive stress levels. The obtained result is especially remarkable since the tested samples have a l/d of 3.0 which allows for free lateral deformation in the central parts of the specimens in the compression test.

A quick literature survey in readily available standard literature (Neville 1994, Ljungkrantz et al. 1994) revealed that, as expected, long-term loading results commonly in reduced compressive strength. Long-term compressive strength is reported to be approximately 80 % of the short-term strength. That is also the commonly used value for structural calculations. However, the actual test method is somewhat different. Here, specimens were loaded for a long time. After that, the actual compressive strength was determined in a short-term test. Within the limited context of this report, it cannot be determined whether or not this explains the observed strength increase. A deeper literature search or additional experiments would be required.

Table 5-2. Compressive strength (cylinder) of creep samples and reference samples from creep test.

Sample ID	Sample type	f_{cc} (MPa)	Avg. f_{cc} (MPa)	s (MPa)
*Grupp1 Ref1**		*69.60*		
*Grupp1 Ref2**		*59.53*		
*Grupp1 Ref3**	***Reference samples TR1* Ø 100 × 300**	*54.44*	*60.75**	*5.81**
*Grupp1 Ref4**		*62.75*		
*Grupp1 Ref5**		*57.41*		
Ref 11		68.10		
Ref 12		72.23		
Ref 13	**Additional reference samples TR1 Ø 90 × 270**	68.98	69.80	1.54
Ref 14		69.71		
Ref 15		70.00		
Grupp2 Ref6		78.08		
Grupp2 Ref7		72.15		
Grupp2 Ref8	**Reference samples TR2 Ø 100 × 300**	79.26	76.79	2.72
Grupp2 Ref9		77.18		
Grupp2 Ref10		77.26		
Grupp3 1		80.44		
Grupp3 2		78.70		
Grupp3 3	**Creep samples TR1a Stress level 40 % of f_{cc} Ø 100 × 300**	76.74	79.38	1.73
Grupp3 4		81.18		
Grupp3 5		79.82		
Grupp4 6		77.98		
Grupp4 7		73.72		
Grupp4 8	**Creep samples TR1b Stress level 50 % of f_{cc} Ø 100 × 300**	81.46	78.30	3.08
Grupp4 9		77.51		
Grupp4 10		80.83		
Grupp5 11		86.53		
Grupp5 12		85.19		
Grupp5 13	**Creep samples TR1b Stress level 75 % of f_{cc} Ø 90 × 270**	87.16	86.65	1.09
Grupp5 14		86.27		
Grupp5 15		88.11		

* Low values and large spread observed. Most likely due to insufficient grinding of the surfaces of the cylinders. Additional samples tested, “Grupp1 Ref1–Ref5” excluded from evaluation.

References

SKB's (Svensk Kärnbränslehantering AB) publications can be found at www.skb.com/publications. SKBdoc documents will be submitted upon request to document@skb.se.

Andersson L, 2018. Kapillärmättnadsgrad. 7C00692-c, RISE Research Institutes of Sweden AB. SKBdoc 1690842 ver 2.0, Svensk Kärnbränslehantering AB. (In Swedish.)

Fjällberg L, 2018. pH-mätning av betongprover från Äspötunneln. 7P00692-b, RISE Research Institutes of Sweden AB. SKBdoc 1690843 ver 2.0, Svensk Kärnbränslehantering AB. (In Swedish.)

Flansbjer M, Magnusson J, 2014. System design of Dome Plug. Creep properties at high stress levels of concrete for deposition tunnel plugs. SKB P-13-37, Svensk Kärnbränslehantering AB.

Grahm P, Malm R, Eriksson D, 2015. System design and full-scale testing of the Dome Plug for KBS-3V deposition tunnels. Main report. SKB TR-14-23, Svensk Kärnbränslehantering AB.

Ikink J, 2015. Provning av låg-pH betong. 5P00163 A, CBI Betonginstitutet AB. SKBdoc 1690844 ver 2.0, Svensk Kärnbränslehantering AB. (In Swedish.)

Kalinowski M, 2018. Undersökning av betongprover från valvplugg. 7C00692, RISE Research Institutes of Sweden AB. SKBdoc 1690841 ver 2.0, Svensk Kärnbränslehantering AB. (In Swedish.)

Ljungkrantz C, Möller G, Petersons N (eds), 1994. Betonghandbok. Material. 2nd ed. Solna: Svensk Byggtjänst. (In Swedish.)

Magnusson J, Mathern A, 2015. System design of Dome plug. Experience of low-pH concrete mix B200. Material properties from laboratory tests and full-scale castings. SKB P-14-26, Svensk Kärnbränslehantering AB.

Neville A M, 1994. Properties of concrete. 4th ed. Harlow: Longman Group.

Olsson G, 2016. Provning av låg-pH betong. 5P00163 B, CBI Betonginstitutet AB. SKBdoc 1690845 ver 2.0, Svensk Kärnbränslehantering AB. (In Swedish.)

Vogt C, Lagerblad B, Wallin K, Baldy F, Jonasson J-E, 2009. Low pH self compacting concrete for deposition tunnel plugs. SKB R-09-07, Svensk Kärnbränslehantering AB.

VTRC, 2006. Petrographic methods of examining hardened concrete: A petrographic manual. Report FHWA-HRT-04-150, Virginia Transportation Research Council, Charlottesville, Virginia.

Appendix

Photodocumentation of drill cores

All drill cores are shown in the order they are removed during drilling, i.e. the first picture shows the part of the core that was removed first. The left side of the first picture shows the downstream surface of the drill core.

A03

B03

G03


nr 1
nr 2
G04
G04 hr 3

G04

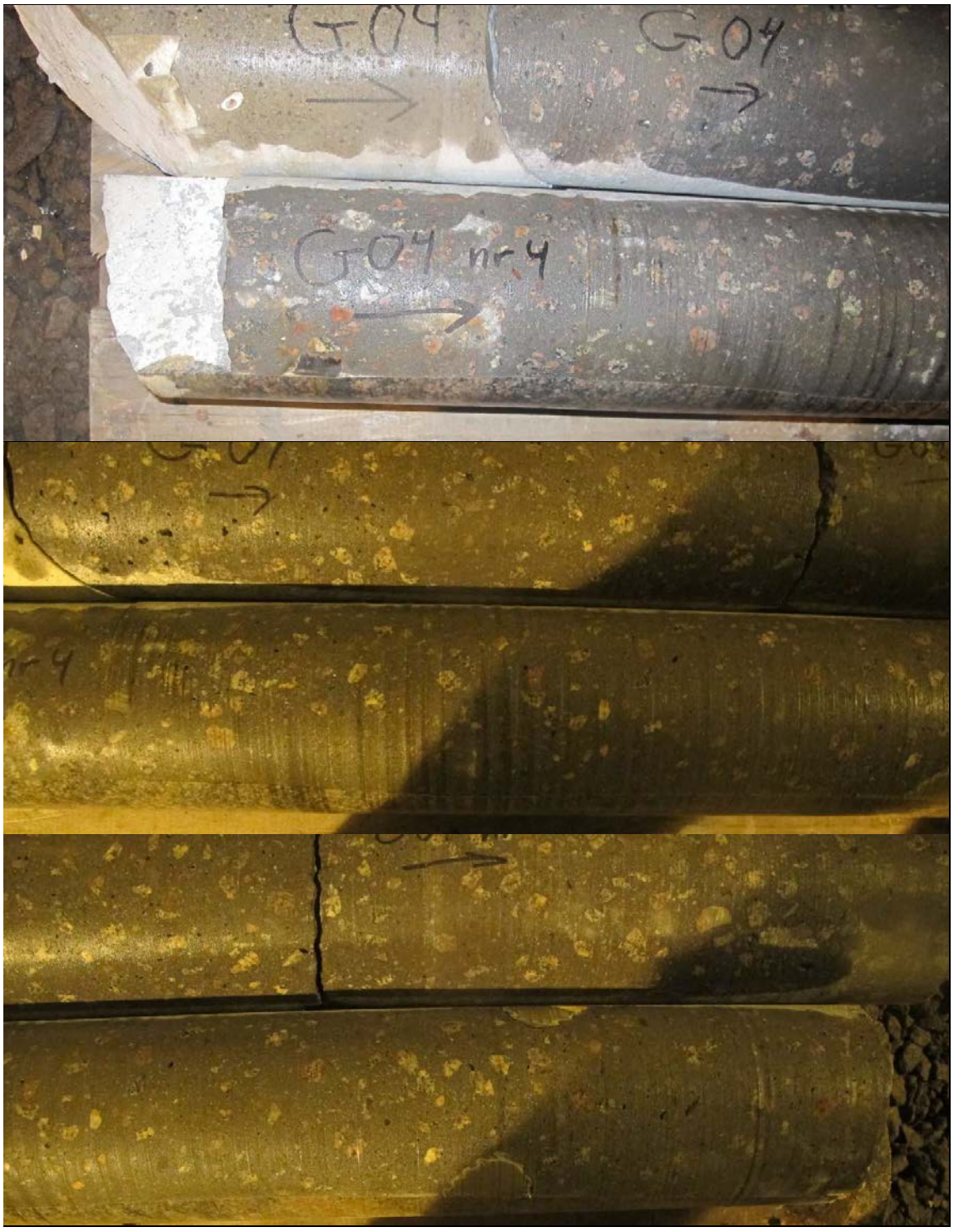
G04
G04
G04 nr 4

H02

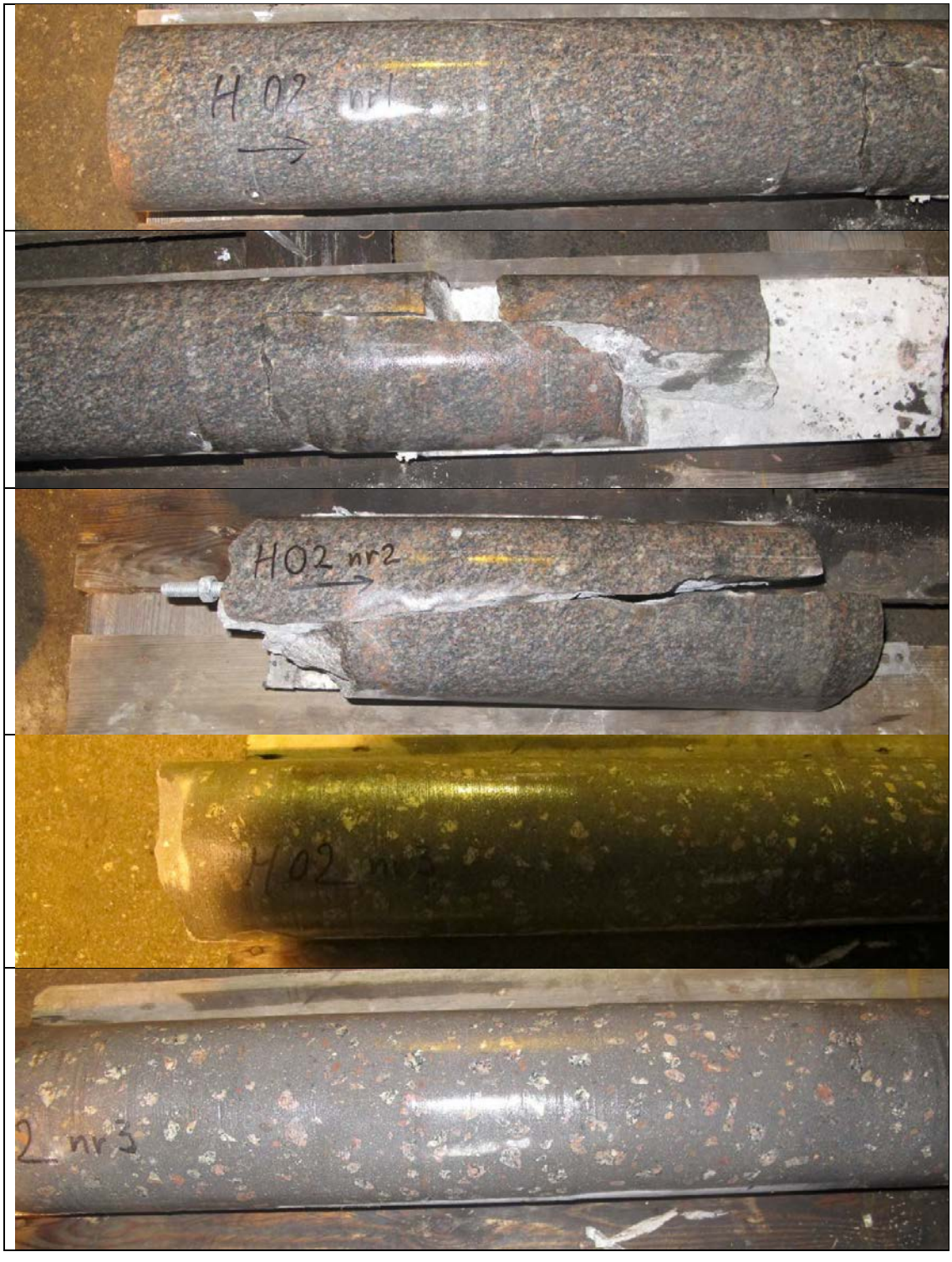

I02

Only the end of the core (close to the slot) is documented.

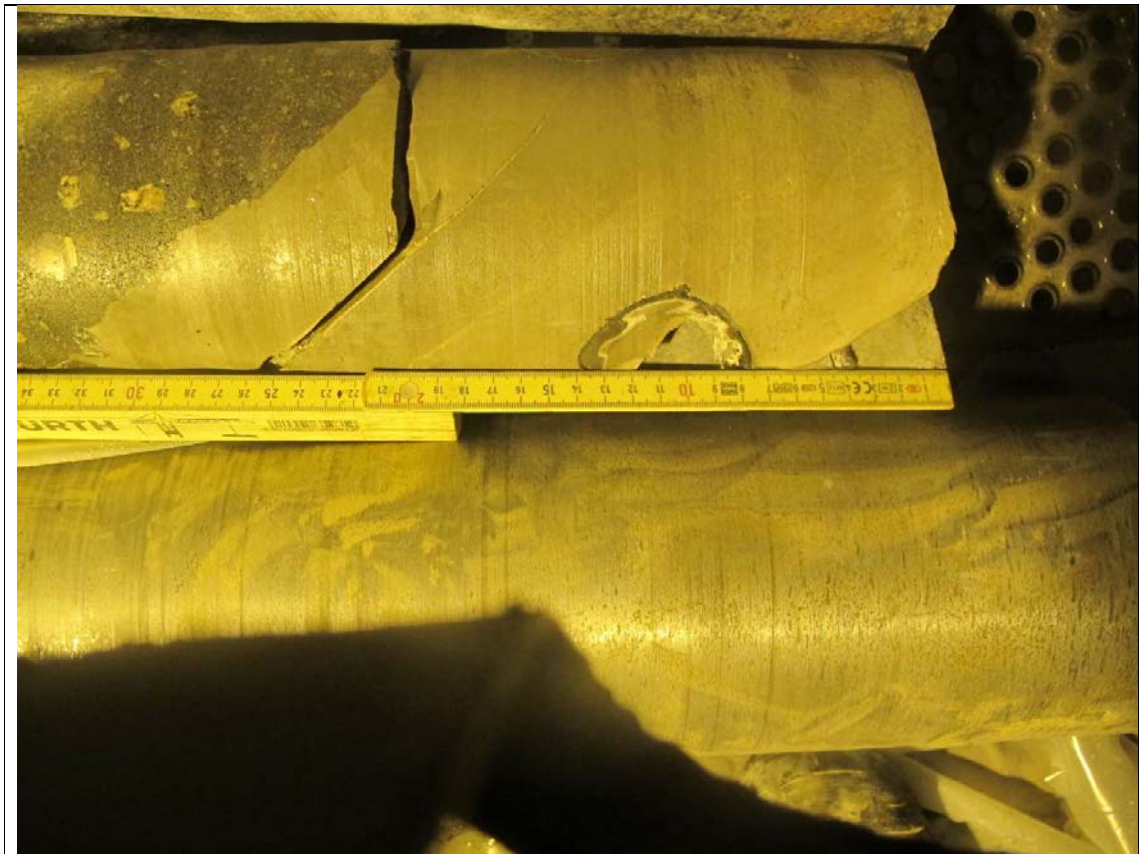

Centrum

Only the end of the core (close to the slot) is documented.

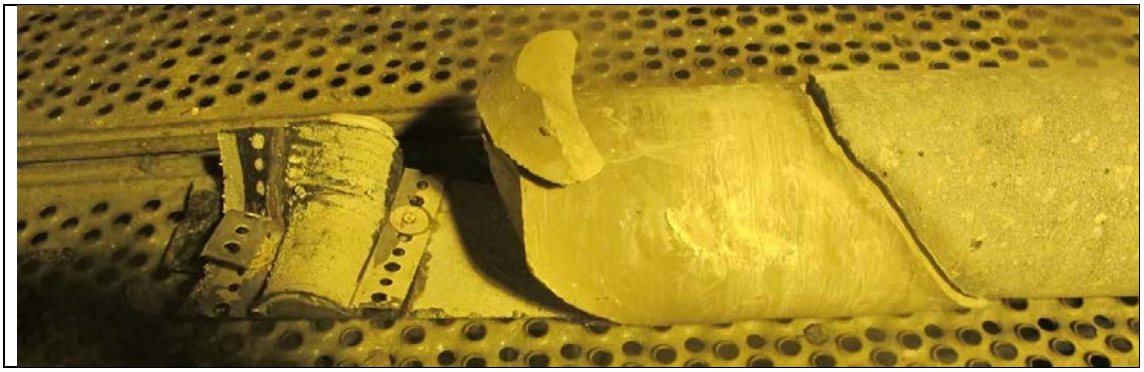

2-1

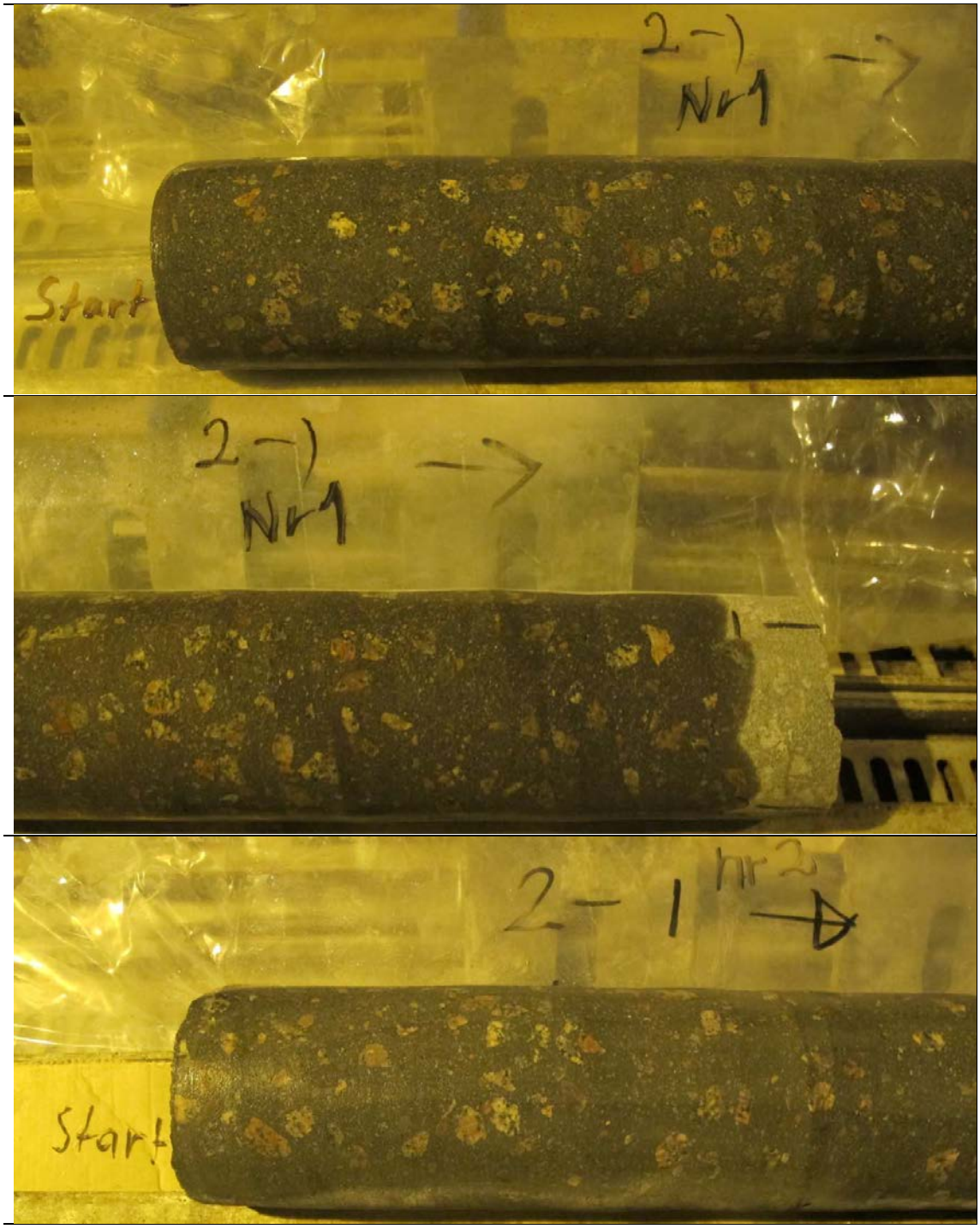

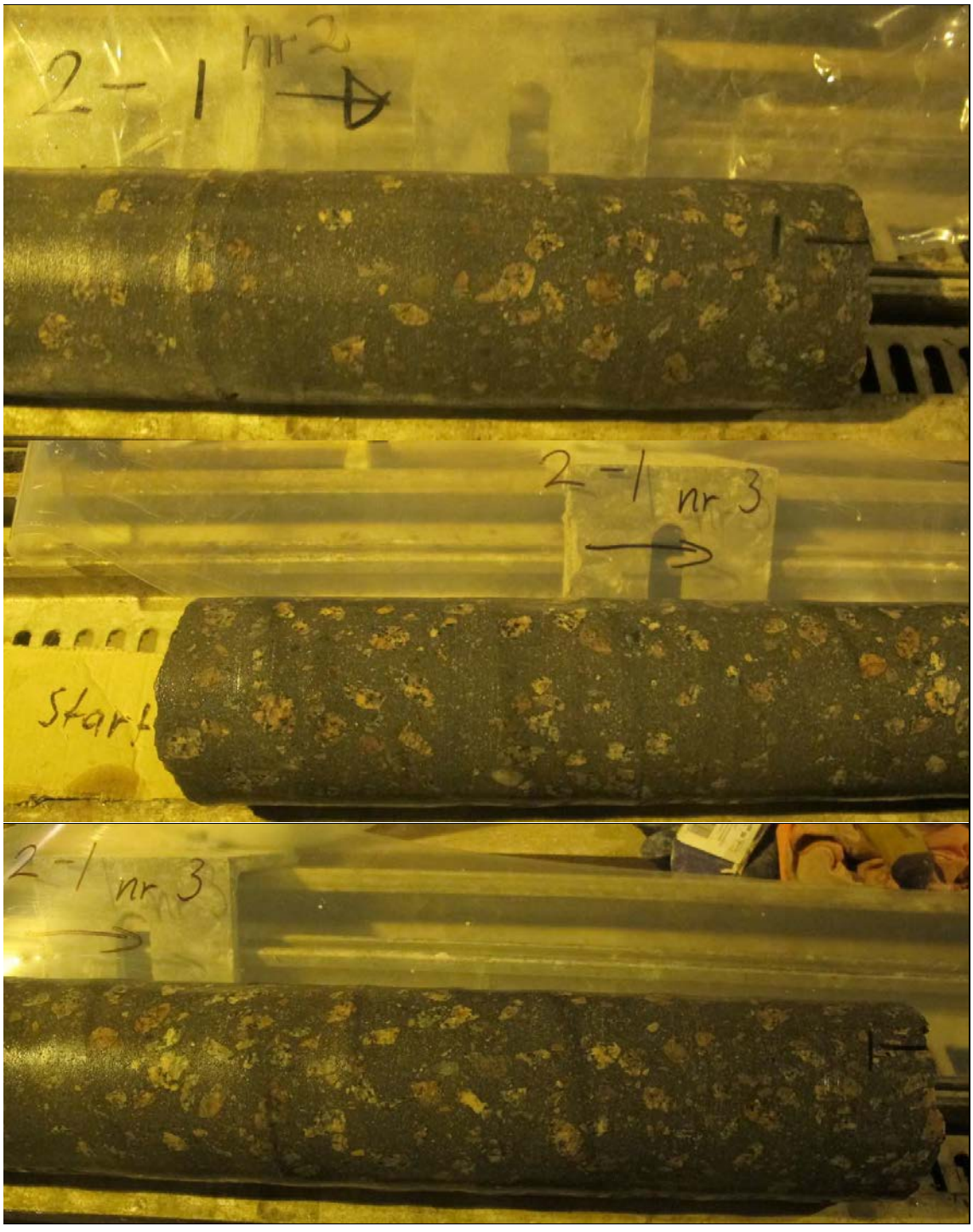
2 - 1 nr 2
2 - 1 nr 3
2 - 1 nr 3


2-2
Nr 1
2-2
Nr 2
2-2
Nr 3
2-2
Nr 4

2-3

2-4

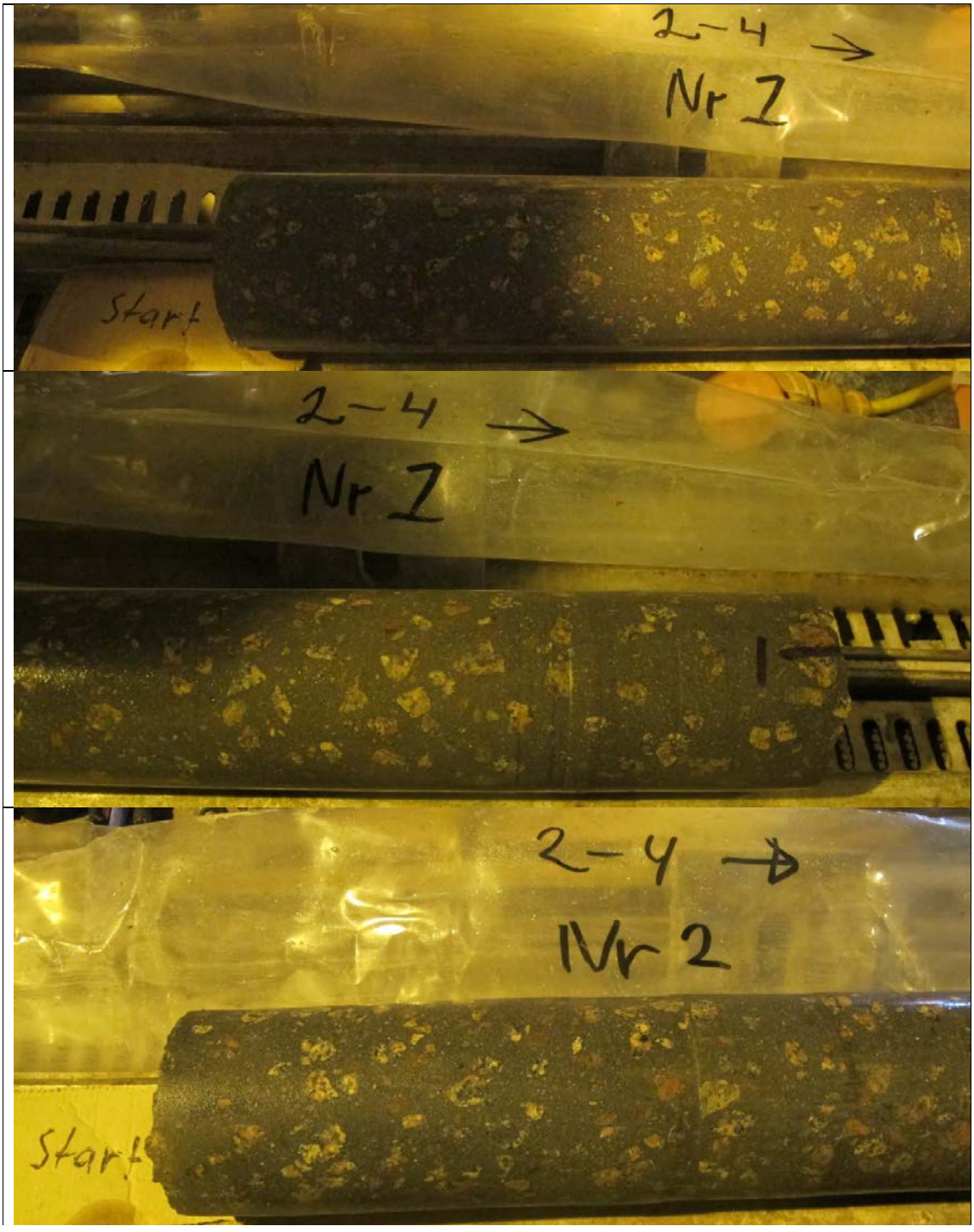

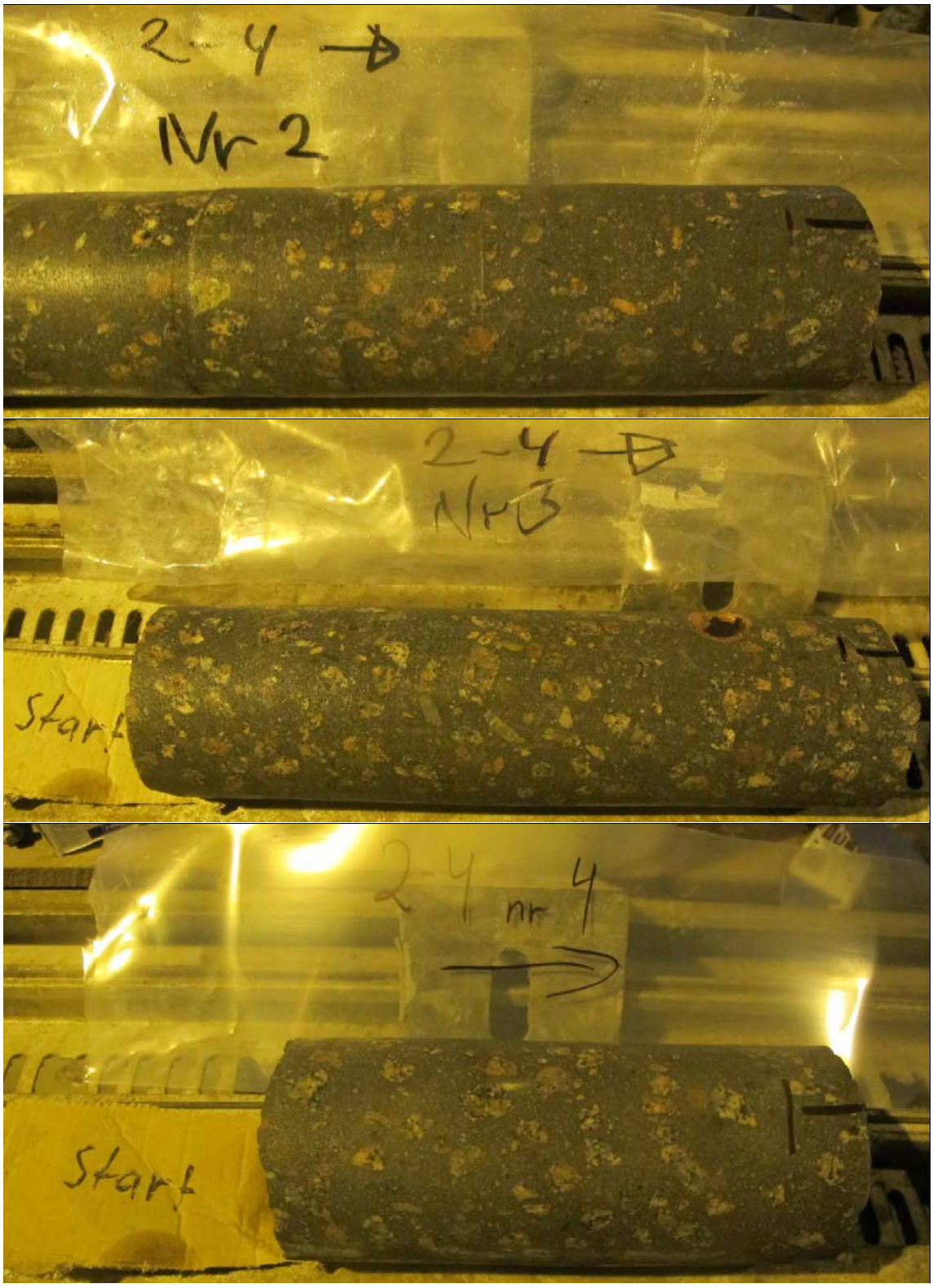
2-4
Nr 2
2-4
Start
2-4 nr 4
Start

3-1

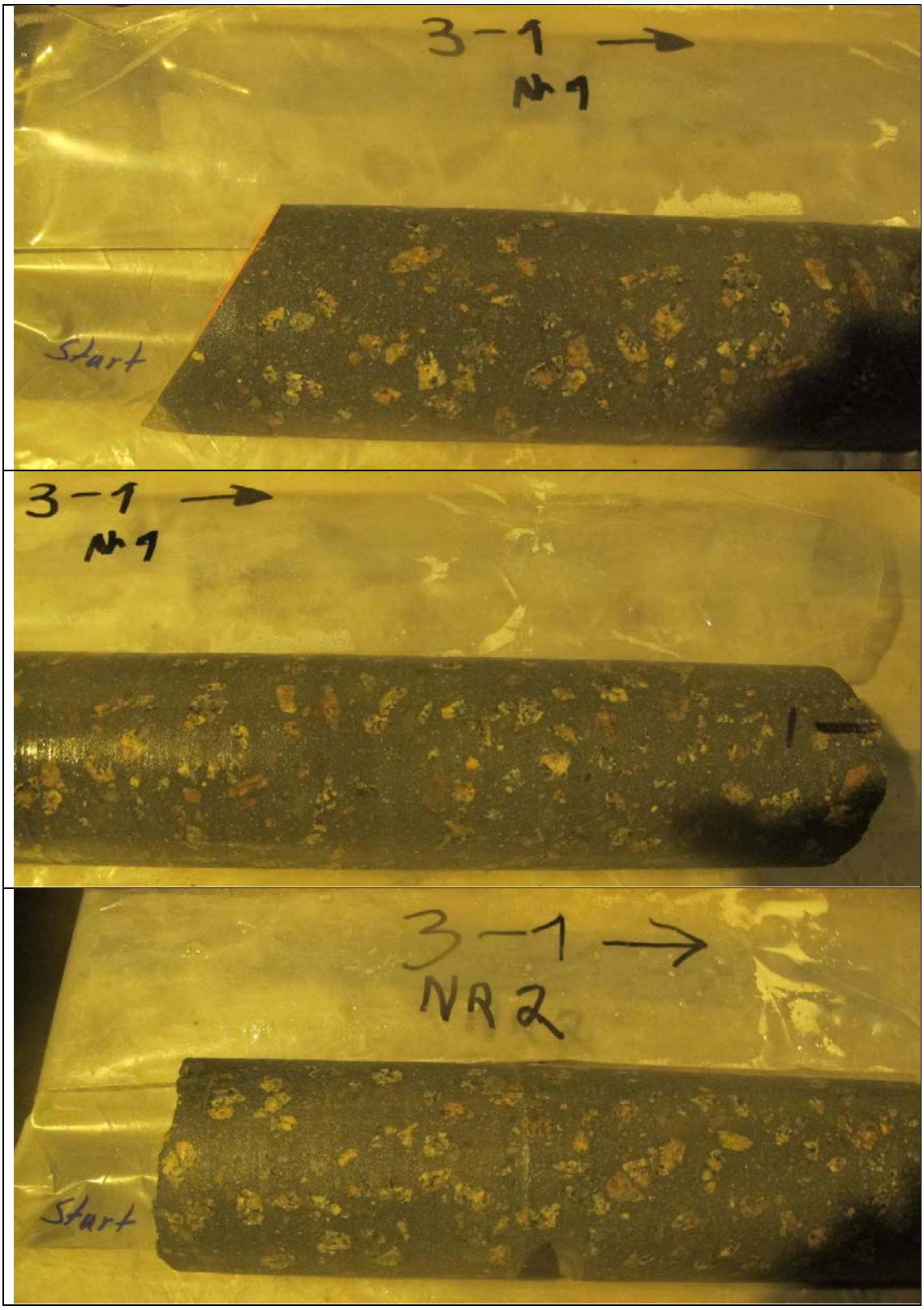

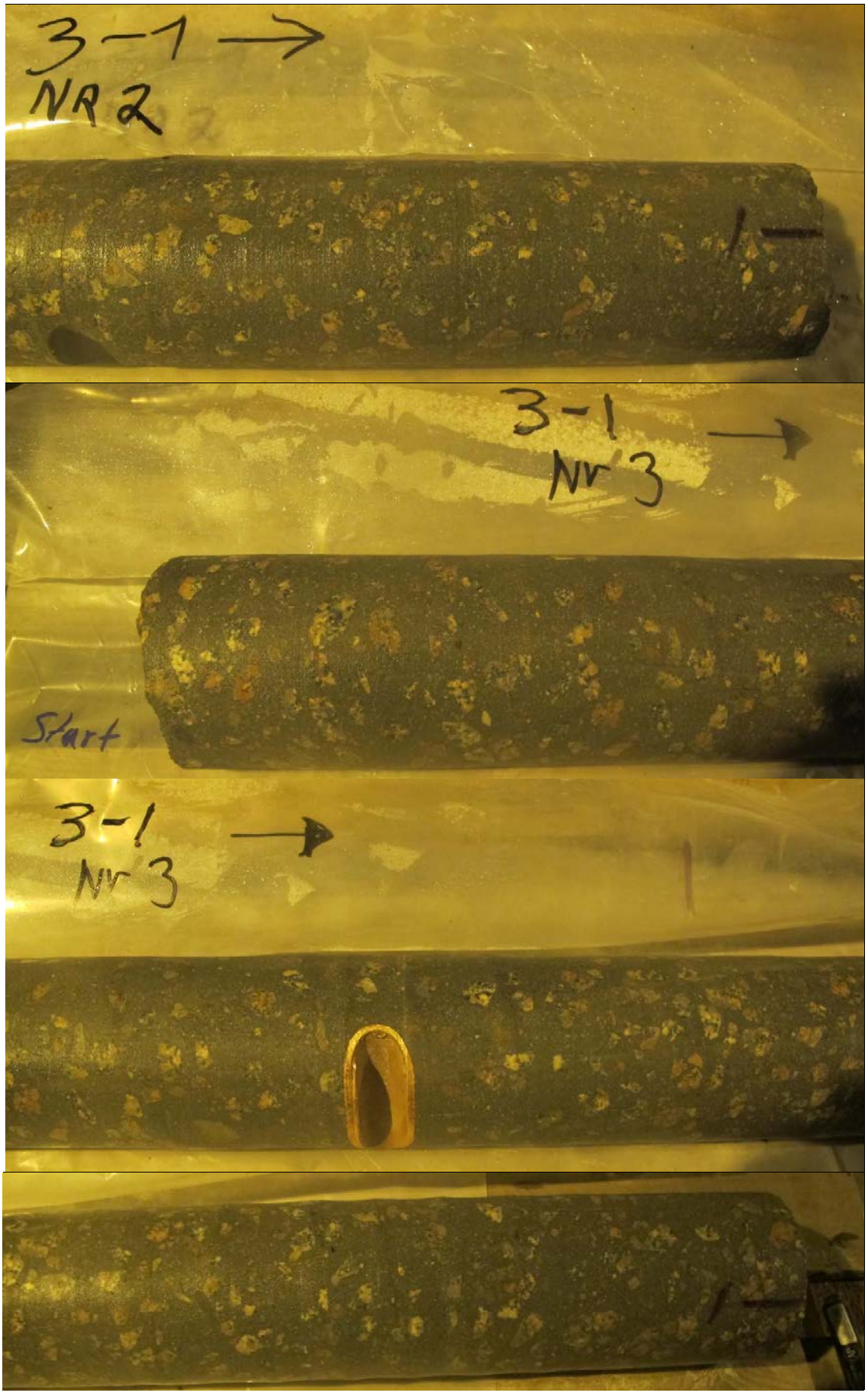
3-1
NR 2
3-1
Nr 3
Start
3-1
Nr 3

3-2

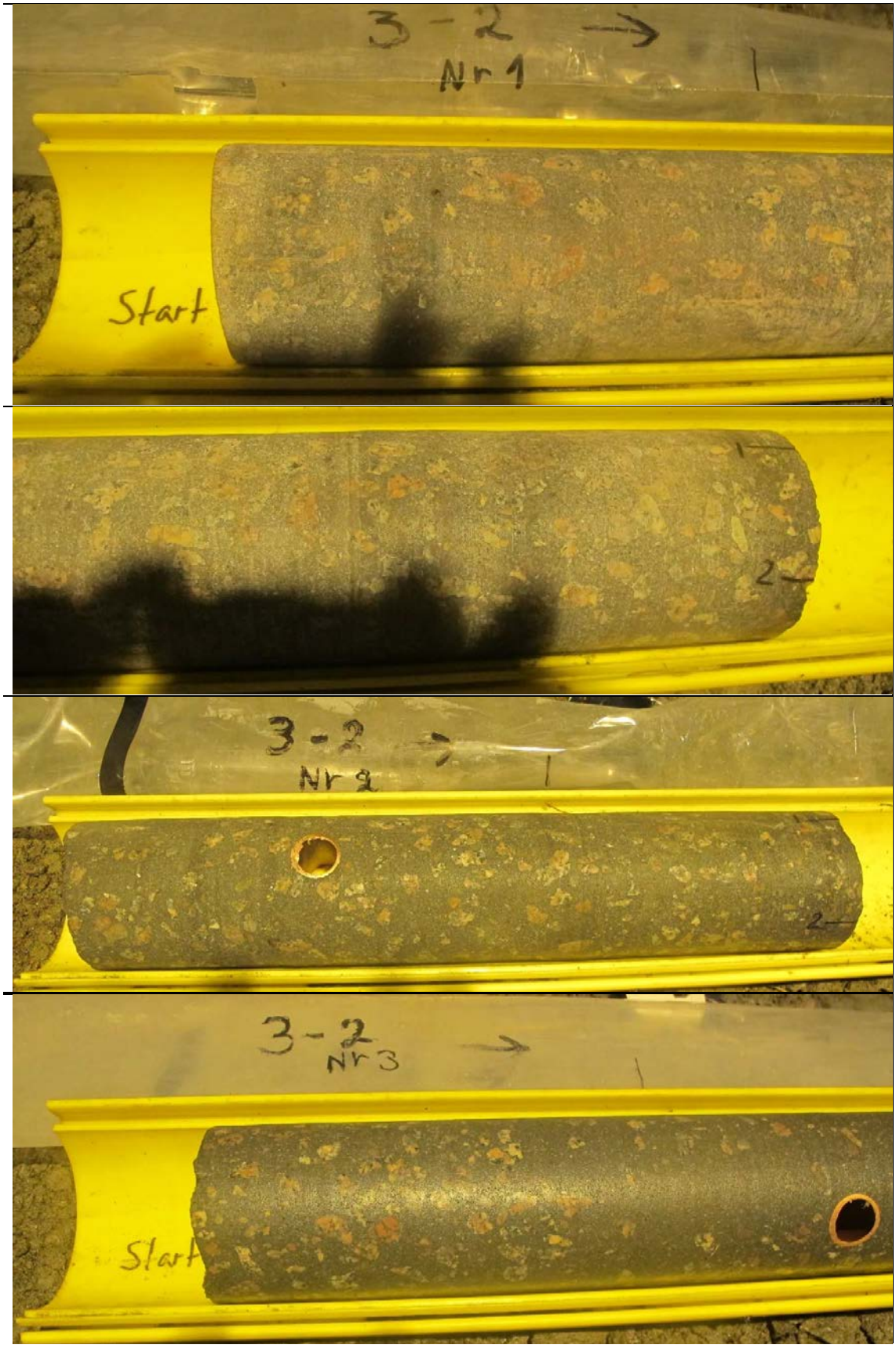

3-3

3-4

Only core parts 3 and 4 documented.

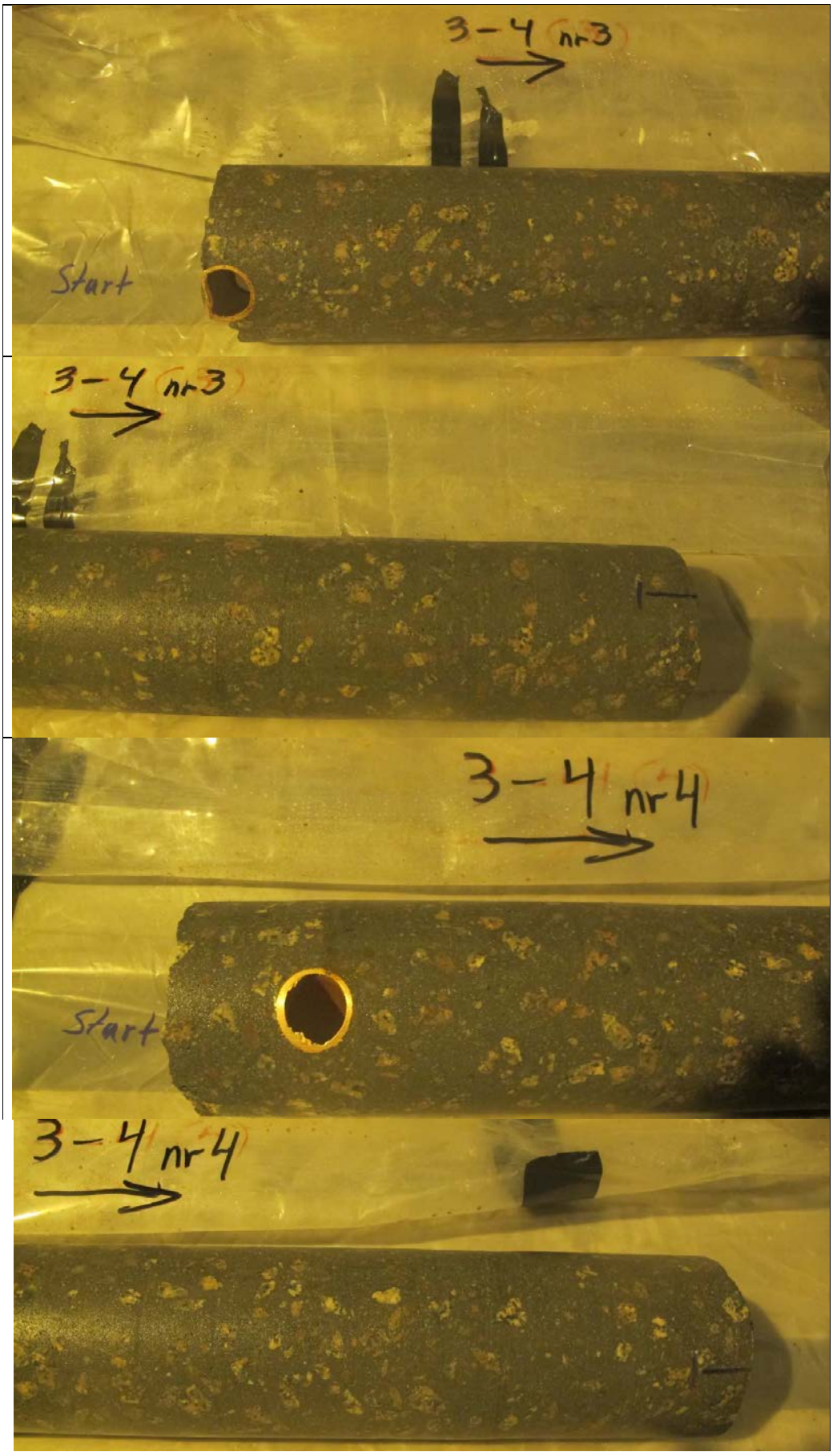

3-5

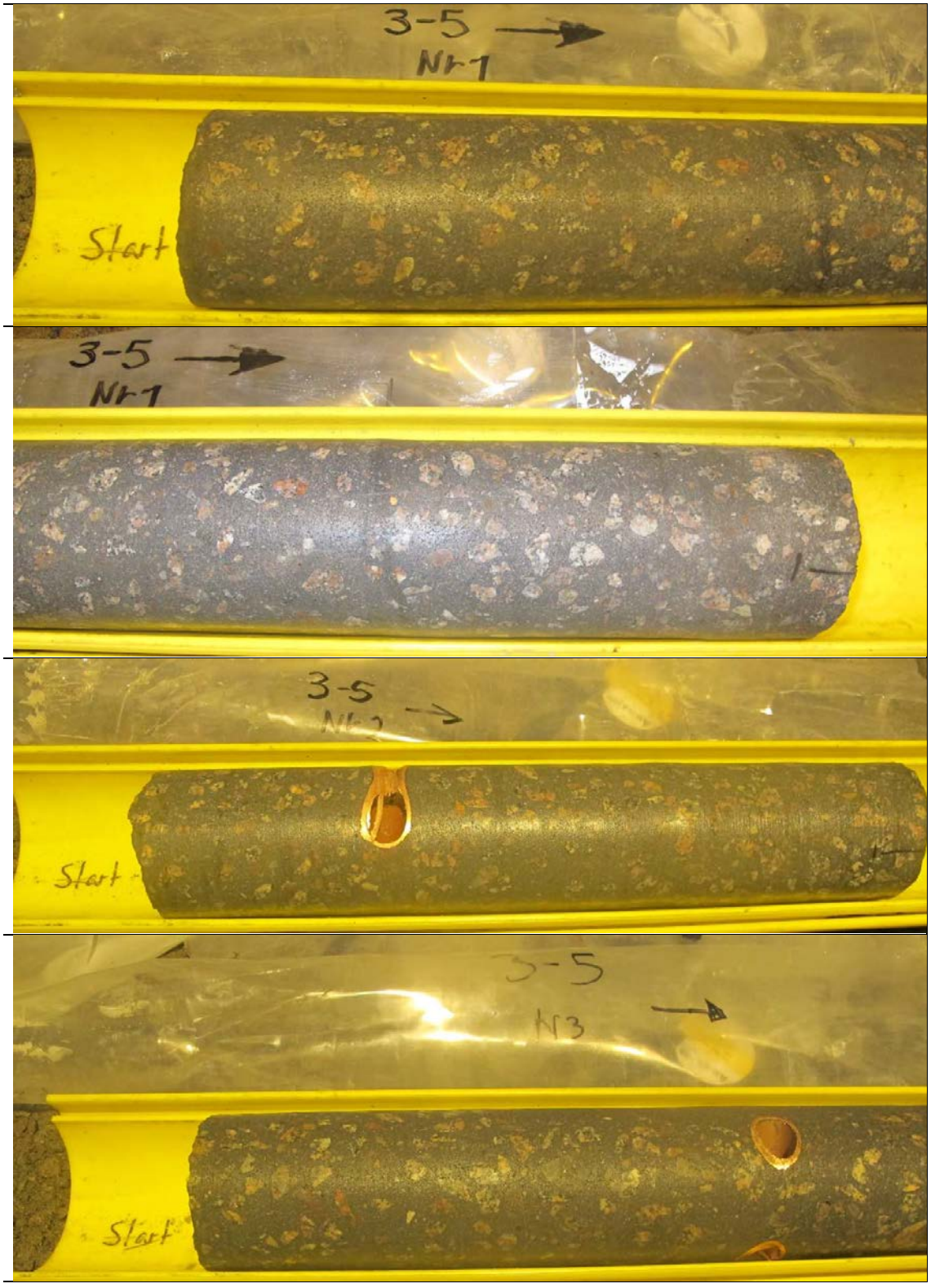


3-5
N3

3-6

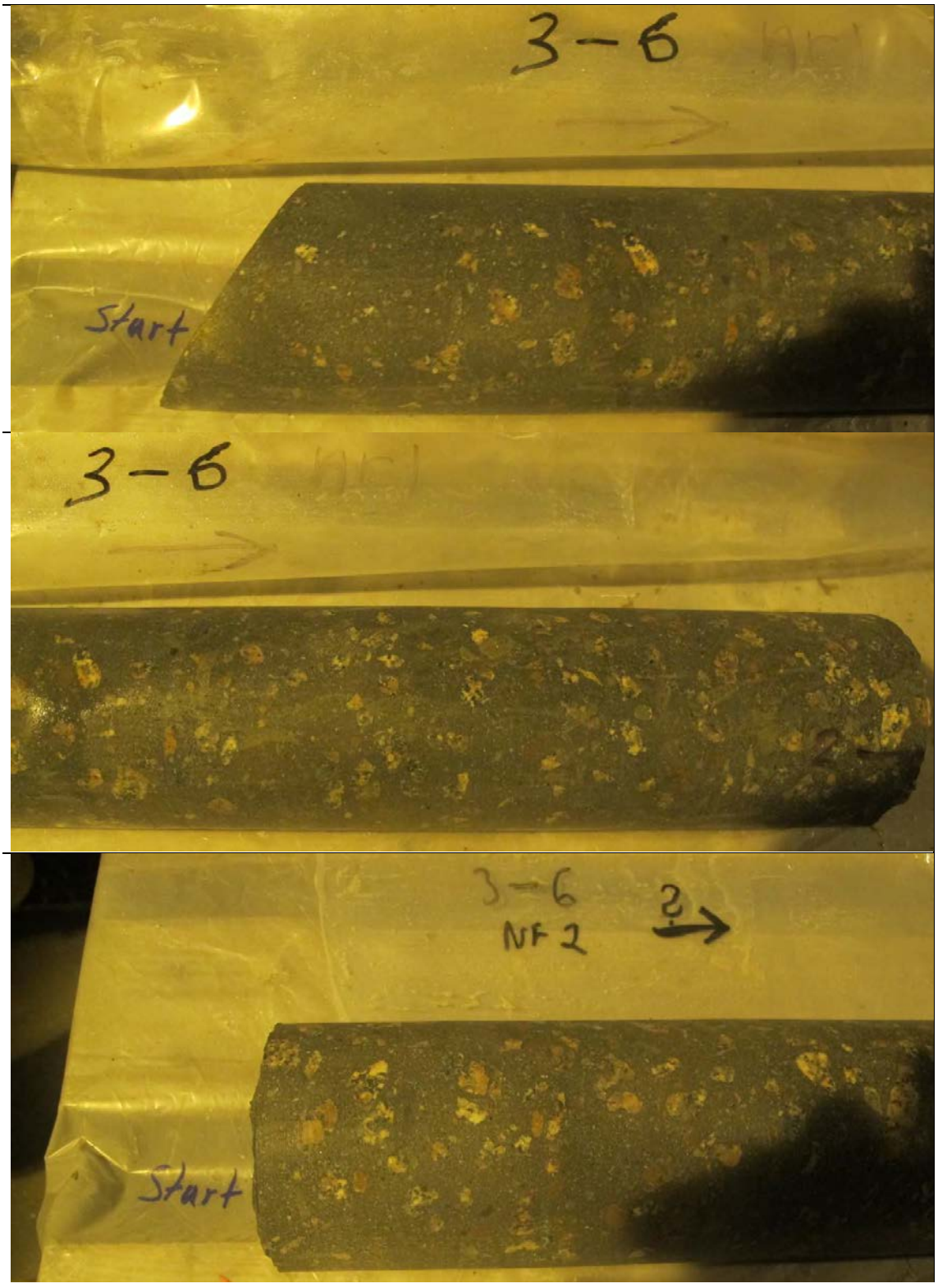


3-6
NF 2
3-6
Nr 3
Start
3-6
Nr 3


3-6
Start
3-6

3-1-1

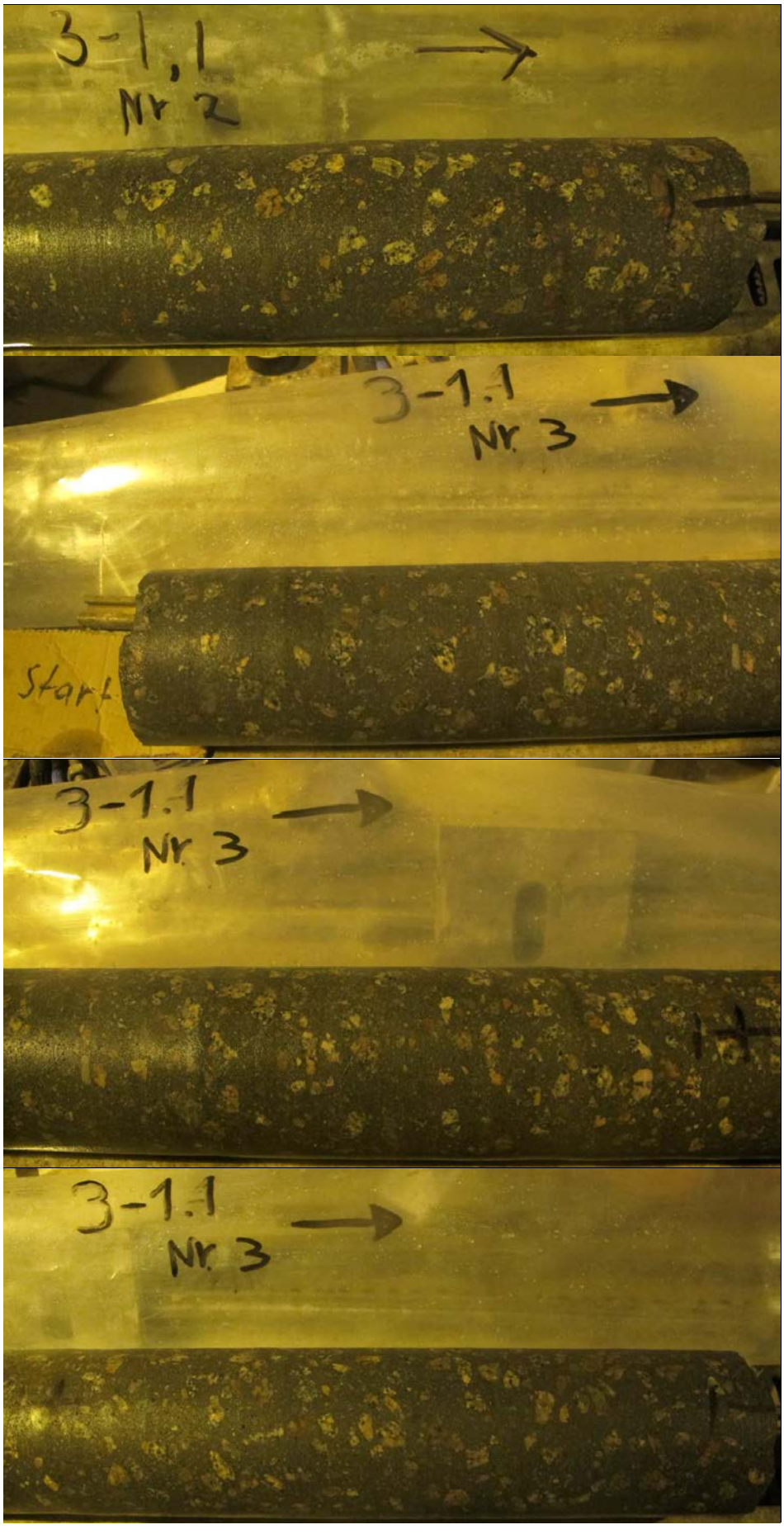
3-1,1
Nr 2
3-1.1
Nr 3
Start
3-1.1
Nr 3
3-1.1
Nr 3

3-2-1

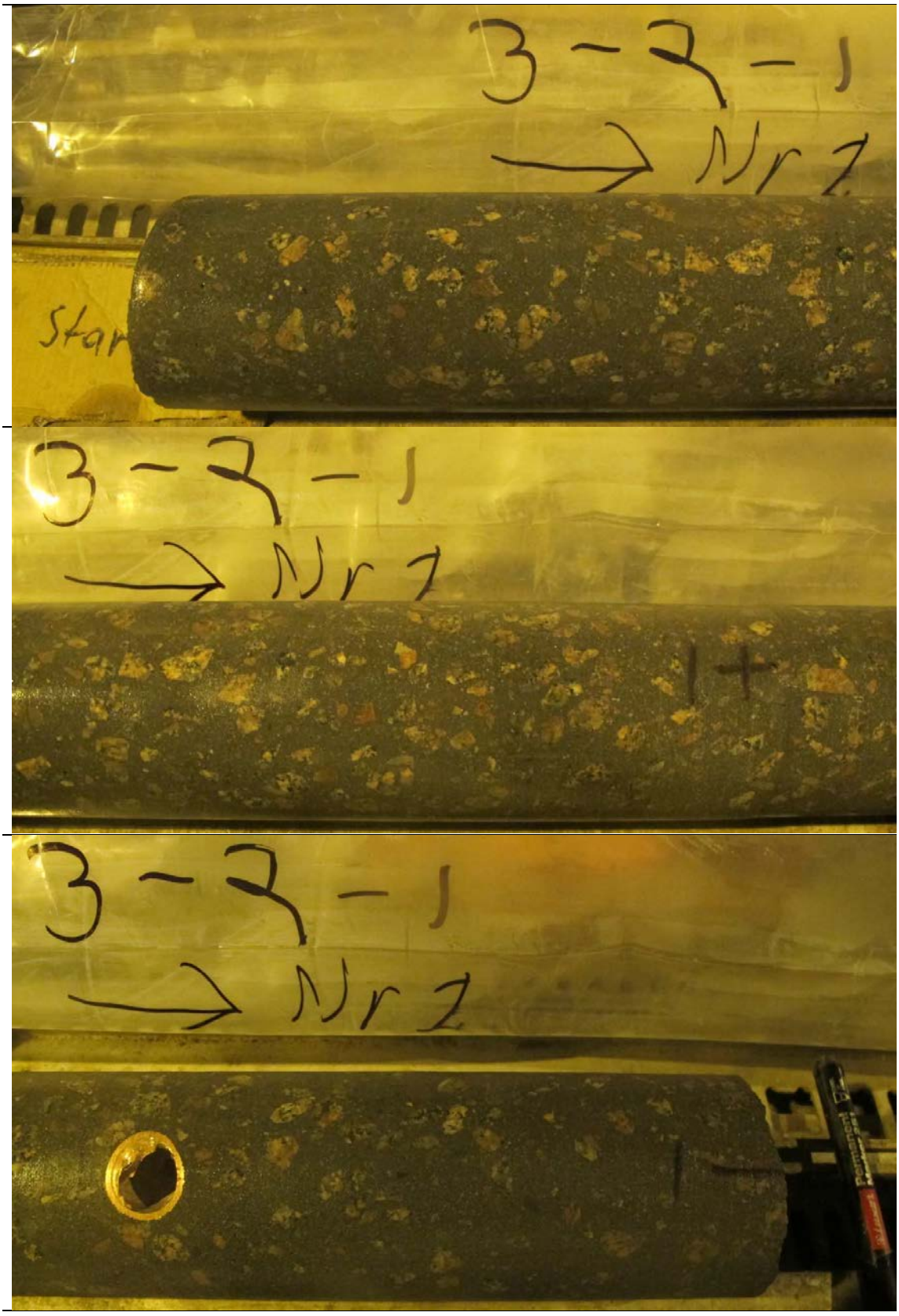

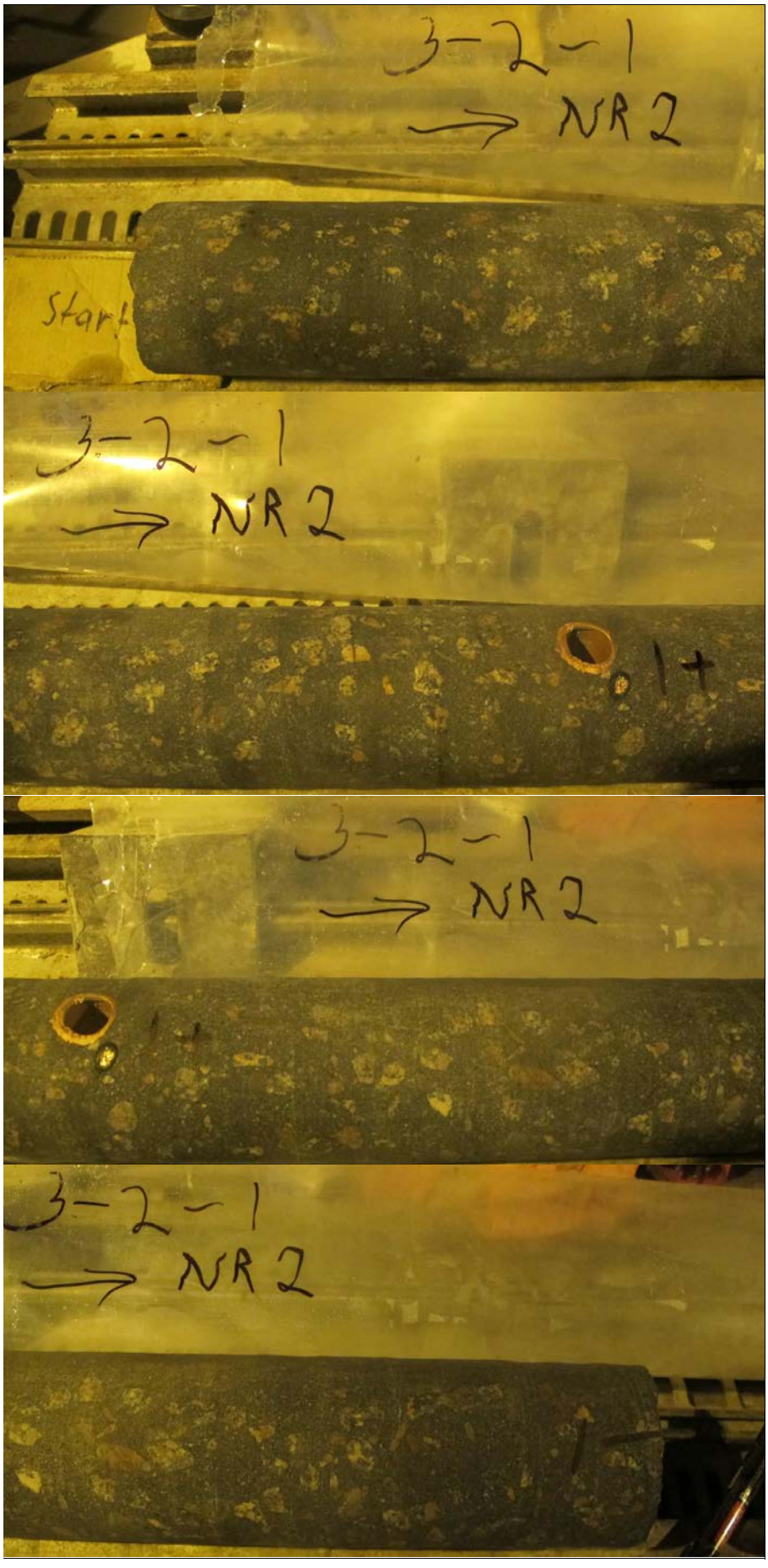
3-2-1
NR 2
Start
3-2-1
NR 2
1+
3-2-1
NR 2
1+
3-2-1
NR 2

3-3-1

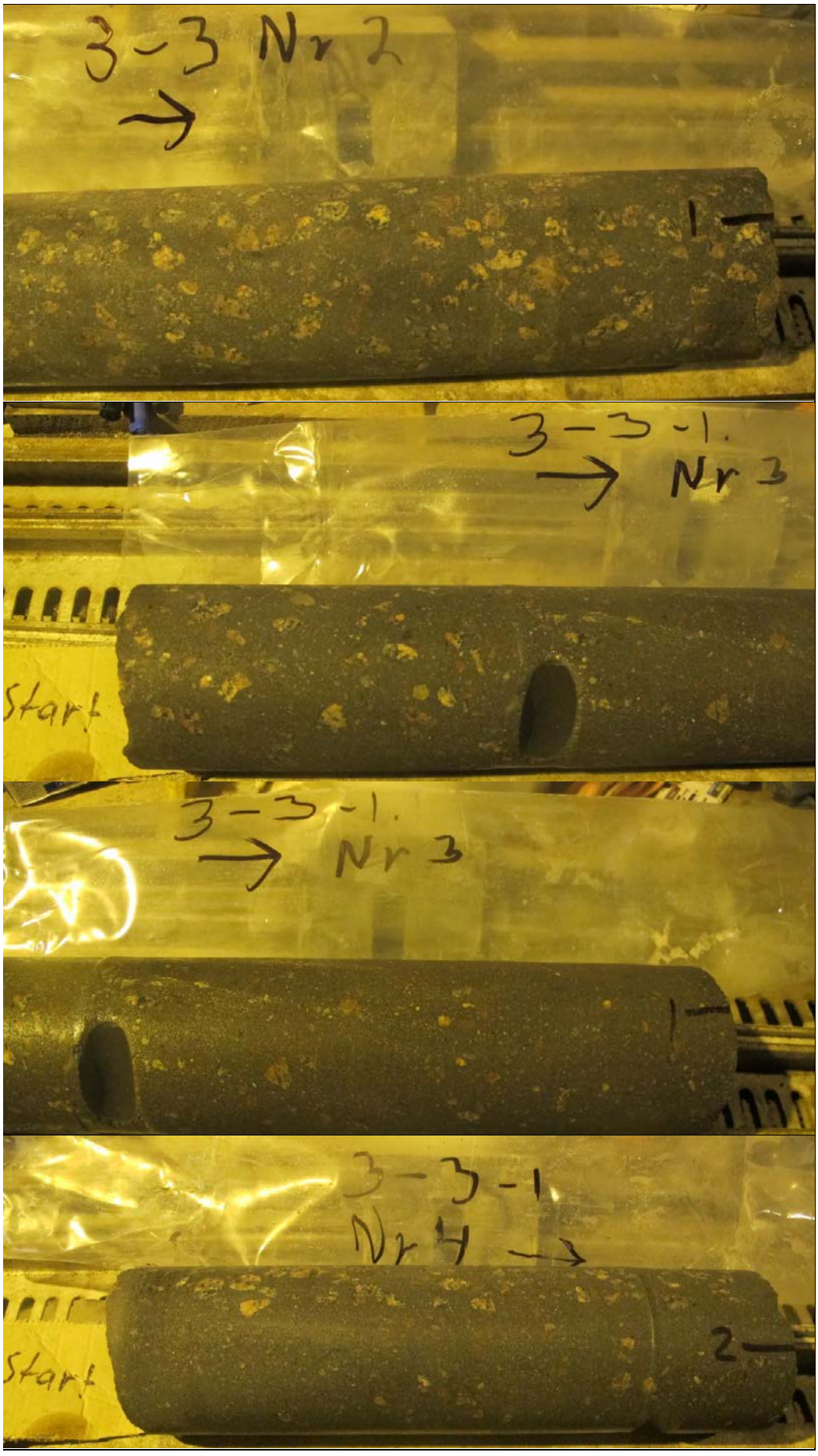
3-3 Nr 2
1
3-3-1.
Nr 3
Start
3-3-1.
Nr 3
1
3-3-1
Nr 4
Start
2
1

Cores from testing in-situ bond strength


POS 4


POS 5


POS 5


POS 5


POS 5


POS 5


POS 6


POS 6


POS 6

Arkitektkopia AB, Bromma, 2019

SKB is responsible for managing spent nuclear fuel and radioactive waste produced by the Swedish nuclear power plants such that man and the environment are protected in the near and distant future.

skb.se